Article

Development of Two-Step Exhaust Rebreathing for a Low-NOx Light-Duty Gasoline Compression Ignition Engine

Praveen Kumar *, Mark Sellnau, Ashish Shah ⓘ**, Christopher Whitney and Rafael Sari**

Aramco Research Center, Detroit, MI 48377, USA
* Correspondence: praveen.kumar@aramcoamericas.com

Abstract: The global automotive industry is undergoing a significant transition as battery electric vehicles enter the market and diesel sales decline. It is widely recognized that internal combustion engines (ICE) will be needed for transport for years to come; however, demands on ICE fuel efficiency, emissions, cost, and performance are extremely challenging. Gasoline compression ignition (GCI) is one approach for achieving the demanding efficiency and emissions targets. A key technology enabler for GCI is partially-premixed, compression ignition (PPCI) combustion, which involves two high-pressure, late fuel injections during the compression stroke. Both NOx and smoke emissions are greatly reduced relative to diesel, and this reduces the aftertreatment (AT) requirements significantly. For robust low-load and cold operation, a two-step valvetrain system is used for exhaust rebreathing (RB). Exhaust rebreathing involves the reinduction of hot exhaust gases into the cylinder during a second exhaust lift event during the intake stroke to help promote autoignition. The amount of exhaust rebreathing is controlled by exhaust backpressure, created by the vanes on the variable nozzle turbine (VNT) turbocharger. Because of the higher cycle temperatures during rebreathing, exhaust HC and CO may be significantly reduced, while combustion robustness and stability also improve. Importantly, exhaust rebreathing significantly increases exhaust temperatures in order to maintain active catalysis in the AT system for ultra-low tailpipe emissions. To achieve these benefits, it is important to optimize the rebreathe valve lift profile and develop an RB ON→OFF (mode switch) strategy that is easy to implement and control, without engine torque fluctuation. In this study, an engine model was developed using GT-Suite to conduct steady-state and transient engine simulations of the rebreathing process, followed by engine tests. The investigation was conducted in four parts. In part 1, various rebreathe lift profiles were simulated. The system performance was evaluated based on in-cylinder temperature, exhaust temperature, and pumping work. The results were compared with alternative variable valve actuation (VVA) strategies such as early exhaust valve closing (EEVC), negative valve overlap (NVO), positive valve overlap (PVO). In part 2, steady-state simulations were conducted to determine an appropriate engine load range for mode switching (exhaust rebreathing ON/OFF and vice-versa). The limits for both in-cylinder temperature and exhaust gas temperature, as well as the external exhaust gas recirculation (EGR) delivery potential were set as the criteria for load selection. In part 3, transient simulations were conducted to evaluate various mode switch strategies. For RB OFF, the cooled external EGR was utilized with the goal to maintain exhaust gas dilution during mode switches for low NOx emissions. The most promising mode-switch strategies produced negligible torque fluctuation during the mode switch. Finally, in part 4, engine tests were conducted, using the developed RB valve lift profile, at various low-load operating conditions. The mode switch experiments correlated well with the simulation results. The tests demonstrated the simplicity and robustness of the exhaust rebreathing approach. A robust engine response, low CNL, high exhaust gas temperature, and low engine out emissions were achieved in the low load region.

Keywords: two-step; dilution; exhaust; rebreathing; light-duty; ultra-low; NOx; GCI

1. Introduction

The imposed regulatory requirements for ultra-low emissions of the criteria pollutants of nitrogen oxides (NOx) and particulate matter (PM) over the CARB SULEV30 [1], Euro 7 RDE [2], and China 6b [3], together with the required 10–15% vehicle fuel economy improvement from 2021 to 2025, are extremely challenging for existing LD engine powertrains. These challenges demand significant engine and aftertreatment (AT) advancements that likely would increase the powertrain complexity and the total cost of ownership. Naturally, the technologies that can deliver ultra-low emissions and competitive fuel efficiency requirements, without major engine re-design and low-cost implications, are among the preferred pathways for engine manufacturers.

One such technology is advanced gasoline compression ignition (GCI)-based combustion recipes [4–10], which offer significant fuel efficiency benefits and low engine-out NOx and PM emissions by applying low intake temperatures, high dilution levels [4–10], and leveraging gasoline's low reactivity to attain sufficient premixed combustion. In the past several years, Aramco's tailored advanced GCI combustion recipe, including a piston bowl, nozzle diameter, # of nozzles, rail pressure, and multiple injection strategy with an appropriate phasing between the pilot and the main injection event, comfortably demonstrated high brake thermal efficiency and very low engine-out NOx and PM emissions for multi-cylinder LD [11–13] and HD engines [14–16]. These demonstrations primarily leveraged optimized fuel stratification distribution for the indicated thermal efficiency gains, while achieving low PM levels from increased air utilization and NOx in the ~1–1.5 g/kWh range using high in-cylinder dilution levels.

While GCI clearly is a cost-effective technology that offers great potential for improving fuel efficiency and emissions, gasoline's low reactivity poses significant technical barriers under low-load operations. Primarily, these risks involve deteriorated combustion stability (high COVIMEP), and higher unburned hydrocarbon (UHC) and CO emissions due to incomplete combustion or near mis-fire events under cold ambient and low-load engine operation. These conditions also reduce exhaust temperature and the risk of severe degradation of the AT system performance. To combat gasoline's low reactivity implications at a low load and under cold ambient engine operations, effective thermal strategies are imperative.

For this purpose, engine-based thermal strategies including retarded fueling, throttling, cooler bypassing, exhaust throttling, spark assistance, and heating devices [17–19], have demonstrated a moderate to high potential for in-cylinder charge thermal promotion, depending on the operating conditions. Nevertheless, owing to their inadequate effectiveness and high fueling penalty trends, engine-based solutions do not quite meet the requirements, thereby requiring effective and fuel-efficient thermal strategies.

For this purpose, variable valve actuation (VVA), by leveraging the variability of the exhaust valve (EV) and the intake valve (IV), offer tremendous potential for in-cylinder charge thermal promotion via the trapping of hot residual gas (RSG), which also offers gas-exchange efficiency improvements when optimized for the engine system.

Previously, VVA strategies such as negative valve overlap (NVO) reported [20,21] significant low-load extension via thermal promotion and optimized fuel stratification in LD engines using partially-premixed mode combustion. However, applying NVO also led to low thermal efficiency attributed to reduced expansion work and high heat transfer losses. As an alternative to NVO, the exhaust rebreathing (RB) valve strategy offered an improved higher thermal efficiency, as a result of the improved gas-exchange process [22,23], for an equivalent thermal promotion potential. However, challenges regarding high smoke emissions with the exhaust rebreathing strategy have also been reported [24–26].

Conventionally, exhaust gas rebreathing refers to partial re-induction of the hot exhaust gases manifold back into the cylinder primarily driven by pressure difference between the cylinder and the exhaust ports, whereas recycling of the exhaust gases by an external pathway is termed as external exhaust gas recirculation (EGR) and involves cooling of the gases to minimize the implications on the engine volumetric efficiency. On the other hand,

exhaust gas rebreathing is regarded as being very effective for charge heating and dilution effects in order to improve robustness and reduce NOx during low load operation.

In recent years, advancements of fuel injection systems, including high fuel rail-pressure capability, have nearly mitigated the high smoke risks, thereby improving the viability of the exhaust rebreathing strategy for GCI-based LD engines. Sellnau et al. [12,22] tested the benefits of a two-step exhaust valvetrain, where the second valve event allowed for the re-induction of hot exhaust gases into the cylinders, which demonstrated a well-promoted, robust, and low UHC and CO emissions for low-load GCI operation. Similarly, Kumar and Zhang [27] reported high effectiveness of the exhaust rebreathing strategy for GCI combustion at a low load, which facilitated a robust combustion process with low NOx and PM emissions at the 10% and 25% load conditions in a heavy-duty engine.

Although previous studies have focused on exhaust rebreathing and its optimization primarily for low-load extension of diesel combustion via thermal promotion, only limited data are reported for GCI combustion under high dilution levels in order to meet ultra-low NOx targets. More importantly, no studies have documented a proper load range criterion for the exhaust rebreathing strategy mode-switch, as well as a transient mode-switch strategy for exhaust rebreathing for GCI, which are necessary in order to pave the way for the practical viability of exhaust rebreathing for low-NOx LDGCI engines. Therefore, this paper focuses on a comprehensive analysis-led development of an exhaust rebreathing strategy for an LDGCI engine from concept stage to the hardware fabrication stage, followed by engine tests.

The investigation study was conducted in five parts, where each part targeted a specific objective and served as a predecessor for the next one. In part 1, a 1D steady-state evaluation was conducted to compare the thermal promotion potential in terms of in-cylinder trapped residual gas (RSG) and the associated gas-exchange losses among different VVA strategies, including exhaust rebreathing (RB). In part 2, a detailed characterization of a family of different RB profiles for RSG vs. fuel efficiency trade-offs was conducted. A proper RB valve profile was conceptualized that was analyzed for the kinematics and hertz criteria compliance for a practically viable cam-lobe profile design. For part 3, using a parametric study, a low-load engine region was analyzed for RB ON→OFF (mode-switch) and vice-versa, whereas in part 4, transient 1D engine simulations were performed, and an appropriate mode-switch strategy was conceptualized that estimated a reasonably smooth engine load transition and low engine-out NOx.

Finally, in part 5, engine tests were conducted using the developed RB cam profile in the low-load region to document the thermal benefits of the exhaust rebreathing and verify potential of the conceptualized transient exhaust rebreathing mode-switch strategy.

2. Engine Setup

In this work, engine tests were conducted for verification purposes. The details of the engine setup and the instrumentations are discussed in the following section.

Engine Setup and Instrumentation

For the engine experiments, a prototype of a four cylinder, 2.6 L, light-duty (LD) gasoline compressions ignition (GCI) engine using the EPA certified E10 Research octane number (RON) 92 gasoline fuel was used. Figure 1 shows the simulated full load curve for the engine, including the low-load region where exhaust rebreathing may be applied.

The engine was equipped with a single stage turbocharger with a variable inlet compressor (VIC) and a variable nozzle turbine (VNT). For cooled exhaust gas recirculation (EGR) delivery, a low-pressure (LP) EGR configuration was utilized. For the intake charge temperature control, a dual charge air cooler (CAC) system was installed. For cold-start assist, an intake air heater was also installed prior to the intake ports. Table 1 shows the key technical details of the engine.
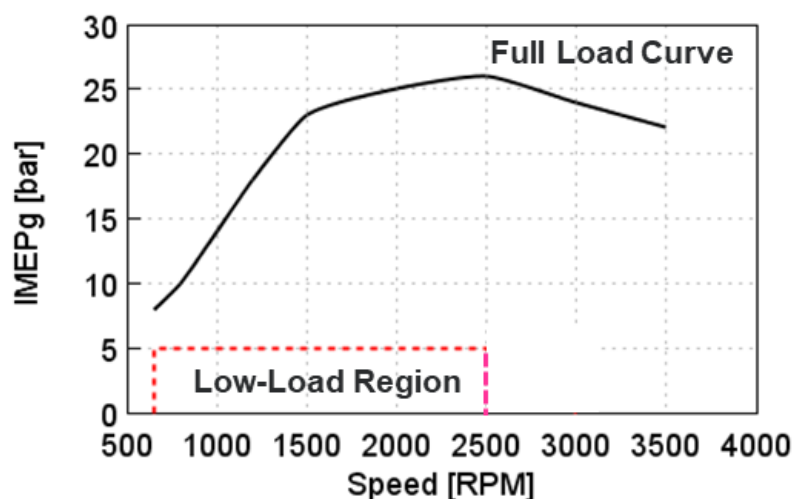
Figure 1. Estimated LDGCI engine load curve and the low-load region.

Table 1. Prototype LDGCI engine details.

Displacement	4Cyl × 0.65 L
Bore/Stroke	82 mm/123 mm
Geometric Compression Ratio	17
Peak Cylinder Pressure Limit	230 bar
Air System	Single-stage VNT turbocharger, with cooled low-pressure EGR system
Charge cooling	Hot and cold charge coolers with a fast blend valve
Thermal Assist	Intake air heater
Valvetrain	Two-step exhaust rebreathing cam

For high-speed pressure data acquisition, a Kistler 6067C piezoelectric pressure transducer (Kistler 6125C) was used in all four cylinders. The sampling resolution was set at 10Hz using a shaft encoder (Kistler 2614A4), and 200 consecutive engine cycles were recorded. The AVL IndiModul hardware and Indicom software package were used for data sampling and processing. Combustion parameters, including the gross indicated mean effective pressure (IMEPg), heat release rate (HRR), and CA50 (crank angle for 50% fuel burned), were estimated from the in-cylinder pressure using real-time sampling. The intake air flow was measured using an AVL Flowsonix Air unit and the fuel flow rate was measured using an AVL FuelExact Coriolis mass flow measurement system. Measures were implemented to maintain cooling of the fuel return cooling for accurate flow measurements. The measurements of the exhaust gas emissions (i.e., NOx, HC, and CO), oxygen concentration, and lambda (λ) were accomplished using an exhaust gas analyzer (Horiba MEXA-7500DEGR) and were converted to the indicated specific values, while the soot emissions were characterized in terms of the filter smoke number (FSN) using an AVL 415SE smoke number meter. The engine was installed with pressure transducers and thermocouples at several locations, including the compressor inlet, the intake manifold, the turbine inlet, the gasoline oxidation catalytic (GOC) inlet, the gasoline particulate filter (GPF) inlet, and at the SCR inlet and the mid-brick locations. At each test point, data were recorded for three minutes after stable engine operation. For the VVA capability, the engine was equipped with a two-step exhaust valvetrain, which included a two-step roller finger follower, hydraulic lash adjuster (HLA), and oil control valve (OCV). Electronic control of the OCV allowed for oil pressure control in HLA, which allowed for a discreet switching ON/OFF mechanism for rebreathing. A detailed technical discussion of the two-step exhaust valvetrain system will be discussed in a separate manuscript.

3. Simulation

In this work, a detailed analysis was carried out using a 1D engine model representing the test engine. The details of the 1D engine model setup and the variable valve actuation (VVA) strategies are discussed in this section.

3.1. 1D Engine Model Details

A GT-Power software [28]-based 1D engine model was developed and calibrated for the analysis. The schematic of the simulated engine setup is shown in Figure 2. The details of the 1D engine model calibration process have been explained previously [19,29] and are summarized here briefly.
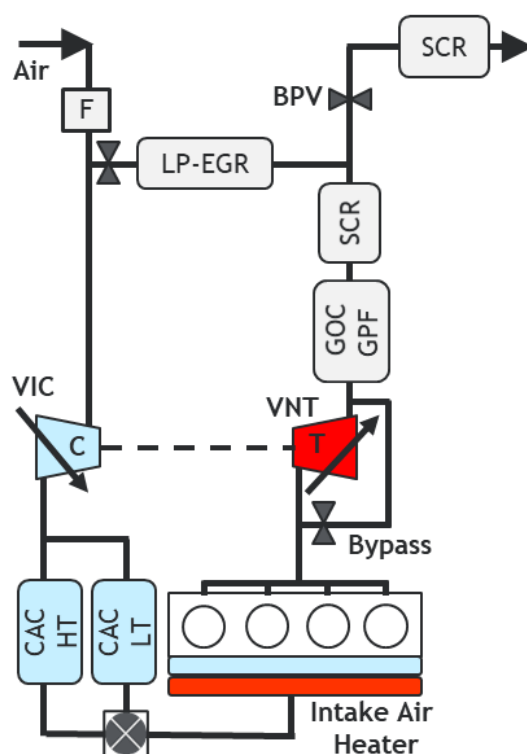

Figure 2. Schematic of the simulated LDGCI engine system setup.

For the air system, a high-efficiency VNT turbocharger including a variable inlet compressor was modeled using the supplier-provided performance maps. For intake air temperature management, a charge air cooler (CAC) design equipped with both high-temperature (CAC HT) and low temperature (CAC LT) pathways, followed by a blend valve, was utilized. A low-pressure EGR (LPEGR) cooling system was configured as a primary strategy for the engine-out NOx control. An exhaust back-pressure valve (BPV) was used to raise the exhaust backpressure, when needed. For the CAC and the LPEGR coolers, fully predictive "master–slave" models were implemented by utilizing corresponding flow-bench data for the coolers. This allowed for capturing the degraded cooling capacity and its implications on the engine performance under aggressive flow conditions. The flow restrictions for the after-treatment (AT) system were also modeled by calibrating an orifice diameter downstream of the turbocharger.

Furthermore, for combustion modeling, a non-predictive heat release rate (HRR) was imposed, including the CA50 (crank angle for the 50% heat release) of 8 crank angle degrees (CAD) and 10–90 (CAD duration between the 10% and the 90% of the cumulative heat release) of 40 CAD. The purpose of the numerical investigation was to analyze and compare the gas-exchange phenomena and dilution level increase potential among different VVA-based thermal strategies. The simplification of the combustion model allowed for comparison primarily based on the gas-exchange penalty, among the VVA strategies, thereby

enabling a logical decision-making process for proper strategy selection. Nevertheless, the testing campaign, discussed in the later section of the study, verified the 1D modeling assumptions, and quantified the in-cylinder and exhaust gas temperature gains, thereby affirming the impracticality of a predictive combustion model development process, for the objectives of this work.

3.2. Variable Valve Actuation (VVA) Strategies

To increase the in-cylinder and the exhaust gas temperatures in the low-load region (shown in Figure 1), different variable valve actuation (VVA) strategies, including (a) early exhaust valve closing (EEVC), (b) negative valve overlap (NVO), (c) positive valve overlap (PVO), and (d) exhaust rebreathing (RB), as shown in Figure 3, were evaluated. Each strategy influenced the quality (in terms of temperature) and quantity of the of in-cylinder trapped residual gas (RSG) using its distinctive underlying gas-exchange mechanism.

For the EEVC (Figure 3a) strategy, fundamentally, advancing of the exhaust valve event allowed for an early blow-down of high-temperature exhaust gases from the cylinder to the exhaust manifold via an early exhaust valve opening (EVO) at the expense of the gross indicated work loss. Consequently, the early exhaust valve closing (EVC) led to recompression of the in-cylinder trapped RSG, increasing the pumping mean effective pressure (PMEP). For this work, up to 40 crank angle degree (CAD) advancing was implemented.

For the NVO (Figure 3b) strategy, the quality and quantity of the trapped RSG, in principle, were expected to be similar to the EEVC strategy, with the advantage of alleviated PMEP levels due to a gradual decline in the in-cylinder pressure from the late intake valve opening (IVO). As a trade-off, late IVO also led to unfavorable cooling of the cylinder charge due to downward piston motion until IVO began. For the NVO strategy, both the EV and IV events were advanced and retarded up to 40 CAD, respectively.

For the PVO (Figure 3c) strategy, the primary mechanism for RSG increase was to increase the cross-flow (reverse flow through the EV and IV) of hot exhaust gases from the exhaust manifold to the intake manifold by retarding and advancing of the EV and IV events, respectively. As a result, the quality of the trapped RSG was expected to be compromised due to a larger expansion of the exhaust gases prior to the cross-flow, and its effectiveness was primarily limited by the physical piston–valve contact constraint. For the simulations, the exhaust and intake valves were shifted up to 30 CAD, within the allowed piston–valve contact constraint.

For the exhaust rebreathing (RB) strategy (Figure 3d), a two-step exhaust valvetrain was simulated, where following the main EV event, a second rebreathe exhaust valve event was triggered during the intake stroke. This event allowed for a reverse induction of the hot exhaust gases inside the cylinders from the exhaust manifold driven by the pressure difference between the exhaust manifold and the cylinder. For this investigation, a family of exhaust rebreathe (RB) valve profiles with the peak lift of 1.8 mm, 2.6 mm, 3.2 mm, and 3.6 mm were investigated. For a moderately aggressive RB profile, a scaled valve profile with a peak lift of 4 mm "RB*4 mm", by imposing similar ramp rates of the RB3.6mm valve profile, was simulated, as shown in Figure 3d. For this family of lift profiles, a mechanical and a hydraulic lash of 0.15 mm and 0.2 mm, respectively, was estimated.

It should be noted that the RB profiles beyond the 4 mm peak lift with similar durations were deemed out of scope due to impractical opening and closing ramps. On the other hand, gradual opening/closing ramps of high peak lift RB profiles would have significantly increased the effective valve area that potentially posed risks for dilution imbalance among the cylinders.
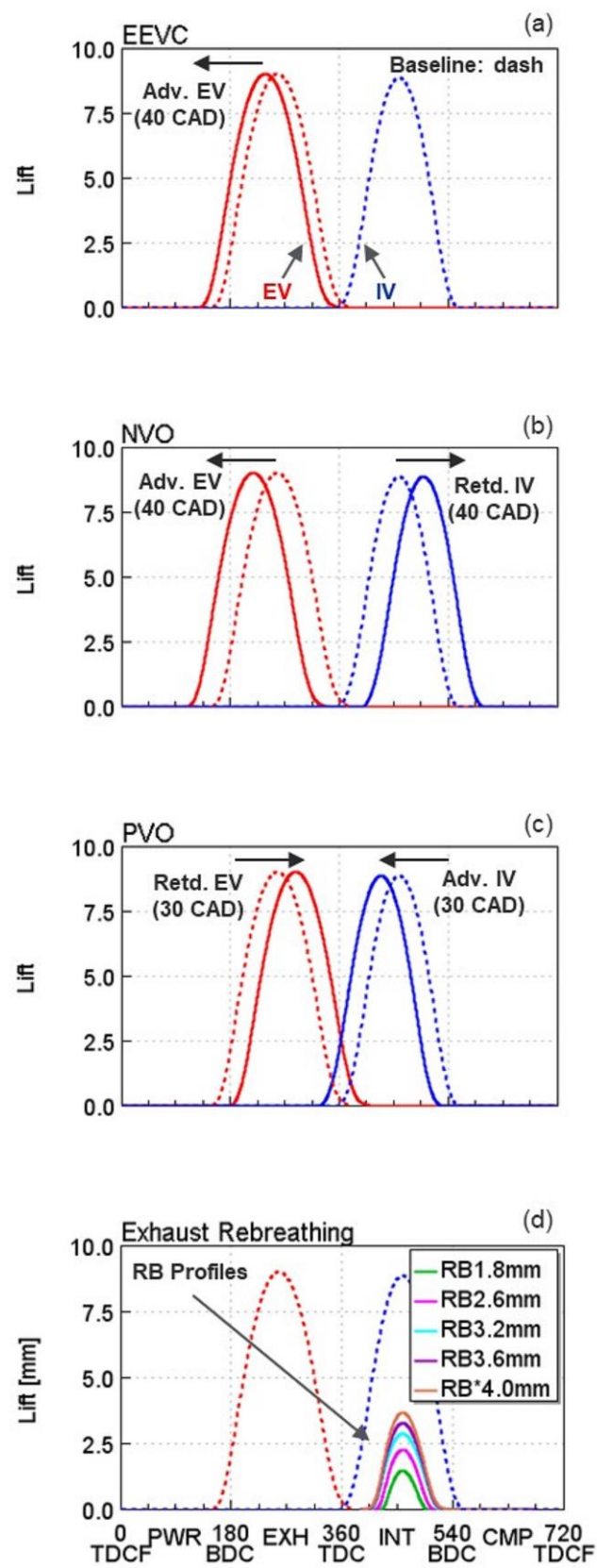
Figure 3. Simulated valve events for the (**a**) EEVC, (**b**) NVO, (**c**) PVO and (**d**) exhaust rebreathing strategies.

4. Results and Discussions

In this section, both numerical analysis and engine test results are discussed. Sections 4.1–4.4 focused on the simulation results. In Section 4.5, detailed engine test results and a correlation with the simulations are reported.

4.1. Simulated VVA Strategies' Performance Comparisons

The VVA strategies' effectiveness were analyzed in the low-load region. The performance of the strategies could be effectively compared in terms of the dilution level increase and the pumping mean effective pressure (PMEP) trade-off. To that end, Figure 4 shows the trends for the total RSG levels vs. the net indicated mean effective pressure (IMEPn) for EEVC, NVO, PVO, and exhaust rebreathing "RB*4 mm" at the 1500 rpm and the gross indicated mean effective pressure (IMEPg) of 2 bar (1500/2) engine condition. The difference in IMEPg and IMEPn is termed PMEP (also known as gas-exchange loss). For each strategy, the turbine rack closing was applied for the RSG increase. For EEVC, NVO, and PVO, the BPV position was maintained as 80% open, in contrast with the 100% open BPV position for the RB*4 mm strategy, owing to its sufficient effective valve area.
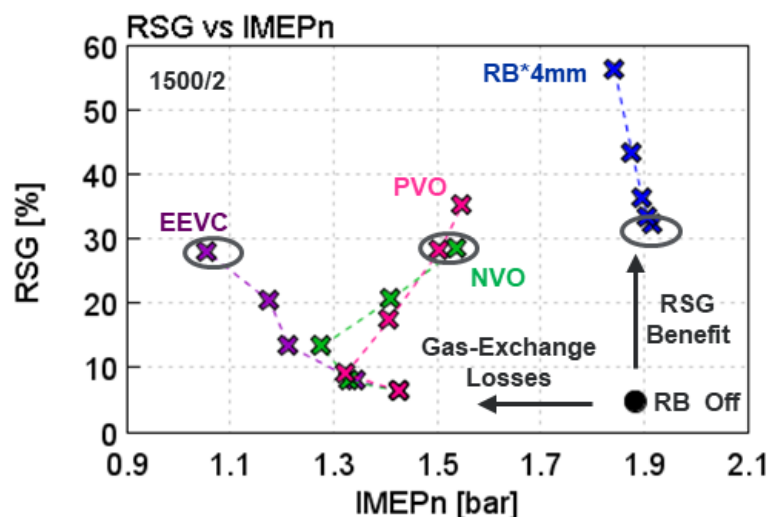

Figure 4. Residual gas (RSG) dilution levels vs. IMEPn trends for different VVA strategies at 1500/2.

As apparent from Figure 4, relatively throttled BPV for the EEVC, NVO, and PVO strategies incurred ~0.5 to 0.6 bar loss in the IMEPn (gas exchange losses) with a marginal rise in the dilution level, from the baseline 1500/2 (no VVA) condition. A significant difference in the RSG vs. IMEPn trends was noticed among the EEVC, NVO, and PVO, owing to the differences in the underlying gas-exchange process among the three strategies. For EEVC, the gas-exchange losses increased proportionally with the increasing RSG level. In contrast, for the NVO and the PVO strategies, IMEPn began increasing with the VNT closing after reaching the RSG levels of 15% and 10%, respectively, indicating a favorable response from the two strategies. Interestingly, the exhaust rebreathing "RB*4 mm" strategy, due to a sufficient effective valve area, t, exhibited a nearly 30% increase in the RSG level without any gas-exchange losses (positive PMEP benefit) from the fully open turbine rack and the BPV, from the baseline. Using VNT closing, the RB*4 mm strategy demonstrated a dilution level potential up to 60% at an expense of merely 5 kPa PMEP increase, compared with the baseline. Table 2 summarizes the predicted PMEP and the exhaust temperature (Exh T) potential for the different VVA strategies. As observed in Table 2, for similar thermal gains, the EEVC, NVO and PVO strategies incurred an additional 0.83 bar, 0.34 bar, and 0.38 bar PMEP, compared with RB*4 mm.

Table 2. Estimated PMEP and Exh T range for different VVA strategies at 1500/2.

VVA Strategies	PMEP (bar)	Exh T (K)
EEVC	$-0.86 \rightarrow -0.95$	508→535
NVO	$-0.86 \rightarrow -0.47$	508→525
PVO	$-0.86 \rightarrow -0.45$	508→535
RB*4 mm	$\mathbf{-0.08 \rightarrow -0.16}$	**522→573**

With the dilution quality differences, the strategies were expected to demonstrate a difference in thermal promotion at a fixed RSG level. To gain insights into each strategy's effectiveness for thermal promotion, in-cylinder temperatures and LogP-LogV trends are plotted in Figure 5a,b, respectively, for the RSG ~30% level. Such a comparison of the cylinder temperature trends among the VVA strategies, while maintaining a fixed HRR and nearly similar dilution level, a condition seldom encountered in engine testing, offered valuable insights for understanding the fundamental valve flow mechanism differences among the VVA strategies.

From Figure 5a, for EEVC, recompression of the trapped RSG, via early EVC, elevated the in-cylinder temperature (Cyl T) beyond 900 K prior to the top-dead-center (TDC) gas-exchange (TDC 360). Subsequently, with the intake valve opening (IVO), the Cyl T rapidly reduced to ~500 K due to reverse flow of the in-cylinder charge through the intake valve. The intake charge further cooled down due to heat losses in the intake ports, thereby leading to a gradual Cyl T reduction trend during the intake stroke and finally achieving the in-cylinder temperature at the intake valve closing (Tivc) of 418 K.

For NVO, while exhibiting an equivalent recompression effect on the Cyl T prior to the TDC 360, the late IVO allowed for cooling down of the trapped RSG from the downward piston motion. While this minimized the undesirable reverse flow of the gases through the intake valve, the Cyl T cooled down ~50 K near the beginning of the IVO. As a result, the NVO strategy displayed a Tivc of 402 K, roughly 15 K cooler than EEVC.

For PVO, the cross-flow of relatively cooler exhaust gases (post expansion stroke) from the exhaust ports to the intake ports momentarily elevated the Cyl T up to 570 K before the TDC 360. Interestingly, the increased heat losses in the intake ports further cooled down the charge temperature, which achieved a marginal Tivc increase of 8 K, from the Tivc of 370 K level for the baseline case. Nevertheless, with the increased induction of the relatively cooler exhaust gases, the RB*4 mm strategy effectively eliminated heat losses in the intake ports by preventing reverse flow phenomena and managed to preserve the rebreathe flow temperature, which steadily raised Cyl T and led to the highest Tivc of 423 K, testifying its superiority compared with other strategies.

From Figure 5b, the LogP-LogV trends clearly displayed the differences in the gas-exchange process among the VVA strategies, at the RSG ~30% level. For EEVC, recompression of the trapped residual gases, from early closing of the exhaust valve, led to high cylinder pressure during the exhaust stroke, resulting in the highest PMEP of 0.83 bar. On the other hand, for NVO, despite an equivalent recompression effect being observed, the late IVO facilitated the expansion of the trapped RSG, thus lowering the cylinder pressure and resulting in PMEP of 0.34 bar. For PVO, higher throttling due to closed VNT caused high cylinder pressure during the exhaust stroke, which led to a PMEP of 0.38 bar, comparable to the NVO strategy. As expected, the RB*4 mm strategy, via unthrottled BPV and VNT positions, managed the PMEP levels event better than the baseline.
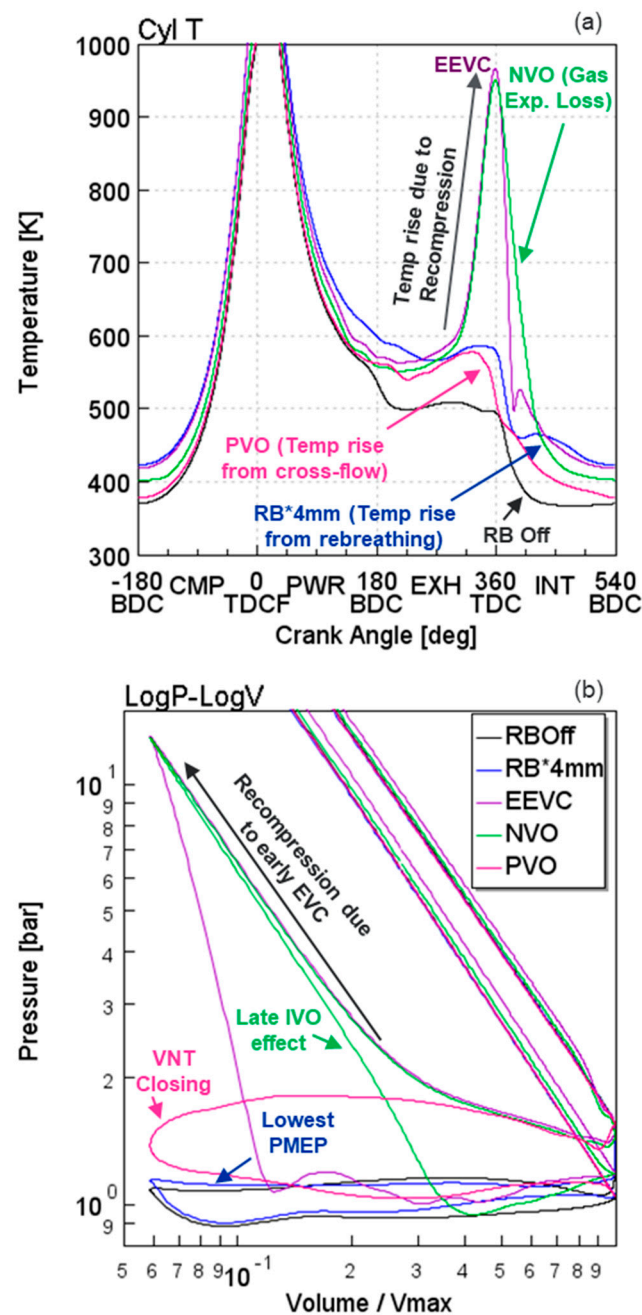
Figure 5. (**a**) In-cylinder temperatures and (**b**) LogP−LogV trend comparisons among different thermal strategies at 1500/2 with a total RSG level ~30%.

To corroborate the observed LogP-LogV trend relevance with the corresponding gas-exchange, the exhaust and the intake valves flows for EEVC, NVO, PVO, and RB*4 mm were examined, as shown in Figure 6. As anticipated, maximum reverse flow through the intake valve was observed for the EEVC strategy, primarily attributed to the recompression effect. The reverse flow was potentially eliminated from the NVO strategy due to a late IVO effect, as suggested previously. For PVO, the valve flow trends demonstrated a dominant cross-flow phenomenon via the reverse flow trend through both the EV and the IV valves. Finally, for the RB*4 mm strategy, no reverse flow trends were observed during the entire engine cycle, thus testifying to its effectiveness for Cyl T and exhaust gas temperatures (discussed in Figure 5a).
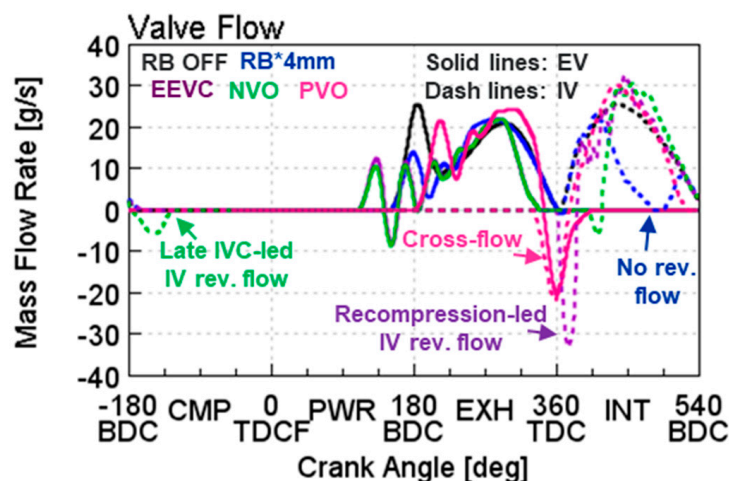
Figure 6. The exhaust valve and the intake valve flow trend comparisons among the EEVC, NVO, PVO, and RB*4 mm strategies at the RSG ~28% level at 1500/2. The RB OFF (baseline) case is also shown for reference.

It is worth mentioning that while these 1D simulations provided valuable insights into the thermal gains vs. gas exchange penalty trade-offs of different VVA strategies, the practical viability of a strategy, based on its complexity, controls, and cost, is equally important. While additional cost and complexity are inherent to all of the strategies, the exhaust rebreathing strategy was judged to be the most suitable to meet the LDGCI engine system requirements.

4.2. Exhaust Rebreathing Characterization

Following the observed effectiveness of the exhaust rebreathing strategy, next, different RB profiles were analyzed (shown in Figure 3d) to characterize thermal potential vs. gas-exchange trends with respect to varying RB lift and duration and identify an appropriate RB profile for low-load operation.

Figure 7a,b shows the RSG vs. IMEPn trade-off trends and corresponding thermal benefits (in terms of Exh T and TDC T increase), respectively, for a family of rebreathe profiles, including RB 1.8 mm, RB 3.2 mm, and RB*4 mm, at two different engine conditions of 650/1 and 1500/2. The RB OFF cases were also plotted for both engine conditions, for reference.

From Figure 7a, the RB 1.8 mm profile, via closing of the VNT and BPV throttling, potentially achieved an RSG level up to 40% at both engine conditions. At 650/1, the IMEPn reduced to 0.89 bar from the baseline 1.19 bar level. The implications on the engine load further increased at 1500/2, where ~IMEPn was noted as ~1.43 bar, from the RB OFF 1.88 bar level. Clearly, at high load and engine speed range, the RB 1.8 mm profile incurred very large high pumping losses due to the relatively smaller valve effective area.

The RB 3.2 mm profile, with a nearly doubled valve effective area, facilitated significantly improved RSG vs. IMEPn trade-off, compared with the RB 1.8 mm profile. The maximum RSG level was achieved at up to ~58%, while improving IMEPn to 0.95 bar and 1.79 bar for the 650/1 and 1500/2 conditions, respectively. From the trends, a larger valve profile was inclined to capture a high residual primarily from VNT closing, and minimized its dilution level sensitivity to BPV actuation. From the engine controls perspective, this offered reduced complexity by allowing for a fixed BPV park position.

As expected, with the largest effective valve area for rebreathing, the RB*4 mm profile showed the maximum RSG and IMEPn benefits at the 650/1 and the 1500/2 engine conditions.
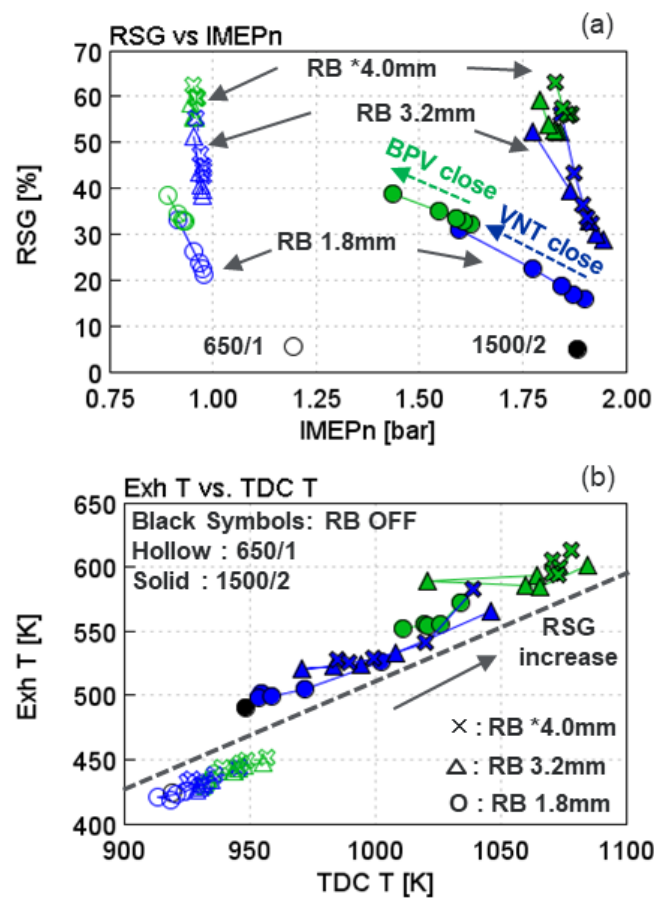
Figure 7. Performance comparisons of RB 1.8 mm and RB*4 mm for (**a**) RSG vs. NMEP trade-off and (**b**) Exh T and TDC T increase for the 650/1 and 1500/2 conditions.

From Figure 7b, because of the increasing RSG levels, the exhaust manifold temperature (Exh T) and the in-cylinder temperature at 10 CAD before the top-dead-center (TDC T), prior to the expected main injection event during the experimental campaign, were examined for different RB strategies at 650/1 and 1500/2. While appreciable thermal promotion of the in-cylinder charge and exhaust gases was observed with the increasing dilution levels, interestingly, the cylinder temperature benefits were consistently larger than the Exh T gains for a given RSG level. This likely resulted from additional heat losses in the exhaust ports and the exhaust manifold attenuating exhaust temperature gains.

Using the RB*4 mm profile, at 650/1 and 1500/2, the maximum temperature benefit was noted as up to 50 K and 100 K, respectively, from the baseline RB OFF cases. The RB 3.2 mm profile showed similar thermal benefits at the expense of higher gas-exchange losses, which further worsened for the RB 1.8 mm profile (shown in Figure 7a).

The re-induction of exhaust gases, for the exhaust rebreathing strategy, were primarily driven by the pressure difference between the exhaust ports and the cylinder ΔP_{EP-Cyl}, which is sensitive to the rebreathing event location relative to the intake valve event. Therefore, to characterize the sensitivity of the rebreathe strategy's effectiveness regarding its location, the performance of the RB*4 mm profile was investigated at three different locations.

Figure 8a–c shows the RB*4 mm profile locations, intake valve flow trends, and LogP-LogV traces, respectively, at 1500/2. From Figure 8a, the simulated locations of the RB*4 mm profile included advanced 30 CAD (Adv30), center (baseline location), and retarded 30 CAD (Retd30), while maintaining the unthrottled BPV and a fully closed VNT position.
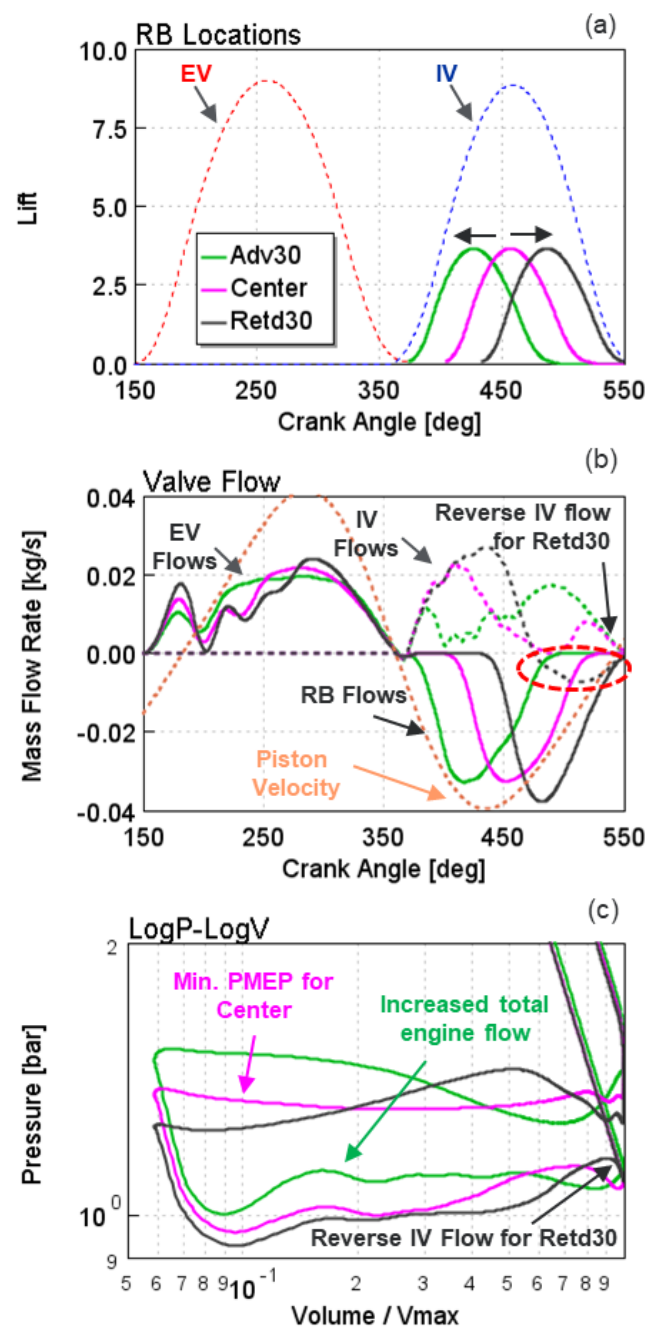
Figure 8. (**a**) Different locations of exhaust rebreathing events, (**b**) valves flow trends, and (**c**) LogP−LogV trends for the corresponding location at 1500/2.

As observed in Figure 8b, a significant difference was noted in the valve flows for the exhaust and the intake valves with varying RB profile locations. For Adv30, the rebreathe flow was reduced by ~2.4%, compared with the center location. This was primarily caused due to reduced ΔP_{EP-Cyl} from the reduced piston speed near the peak lift of the RB*4 mm profile. Consequently, this loss of RSG level led to an increased total engine flow (~10%) that was conjectured to weaken the thermal effectiveness of the strategy and increase PMEP. On the other hand, the induction of the exhaust gases was superior for the Retd30 location during rebreathing; however, the incurred reverse flow due to late closing of the rebreathe valve suffered loss in the RSG level. The center location, due to the synchronized peak RB*4 mm lift with the maximum piston velocity, maximized the trapping of the RSG due to the largest ΔP_{EP-Cyl}.

From Figure 8c, the pumping losses estimated from the gas-exchange loops were noted as being ~1 kPa and 5 kPa higher for the Adv30 and the Retd30 locations, respectively, compared with the center location, thereby highlighting the best performance at the center location. Similar results were also reported in previous studies [12,22,27].

Furthermore, a proper valve location is instrumental in maintaining a low dilution imbalance among cylinders, which is partly dictated by ΔP_{EP-Cyl}, during the exhaust rebreathing event. Figure 9 compares the predicted deviations in the total RSG level in each cylinder from the normalized mean RSG level of all the four cylinders at three different locations. Interestingly, the Retd30 location showed the highest RSG imbalance among the cylinders primarily due to the incurred reserve flow through the intake valve near the IVC, as observed in Figure 8b. No reserve flow phenomena were noted for the Adv30 and the center locations, which exhibited considerable improved RSG balancing. Evidently, the center location resulted in the lowest RSG deviation, thus offering the most balanced RSG distribution among the four cylinders. This was likely facilitated by the largest pressure difference ΔP_{EP-Cyl} from the synchronized peak RB lift with the peak piston velocity, as discussed previously.
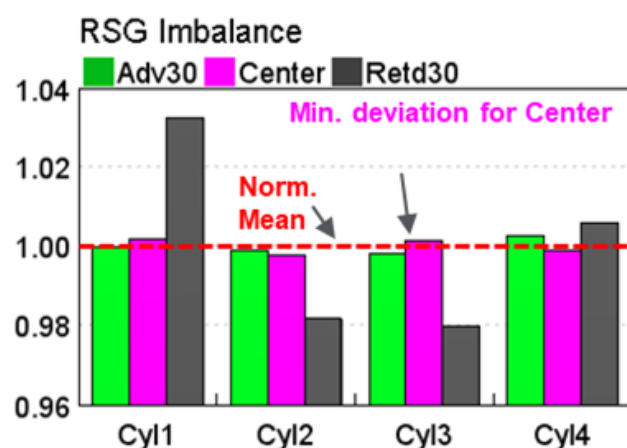

Figure 9. Residual gas (RSG) distribution imbalance among the cylinders for different RB profile locations.

4.3. Load-Range Evaluation for RB Mode-Switch

In-cylinder charge thermal promotion is necessary to improve the combustion robustness and exhaust temperatures in the low-load region. However, thermal promotion becomes less desirable with the increasing engine load due to the risk of a high maximum pressure rise rate (MPRR) and increased engine-out NOx resulting from an overly advanced combustion phasing [12,24,27]. Therefore, for the successful implementation of the exhaust rebreathing strategy, it is imperative to determine an appropriate engine load range where exhaust rebreathing (RB) can transition from ON→OFF (mode-switch) while satisfying the following criteria:

- Avoid excessive MPRR and engine-out NOx during RB ON.
- Maintain adequate cylinder and exhaust temperatures during RB OFF.

To this end, a detailed parametric study involving VNT and BPV positions was conducted for the IMEPg range of 2–7 bar at an engine speed of 1500 RPM, for both RB OFF and RB ON cases, using the RB*4 mm profile. Figure 10a,b shows the range of the simulated VNT and BPV positions, respectively. The VNT position range was implemented from 1 (fully open) to 0.05 (nearly fully closed), remaining more skewed toward closing positions to achieve high dilution levels during rebreathing, as shown in Figure 10a. For BPV, from Figure 10b, two positions were included at 0.8 (80% open) and 0.5 (50% open). More aggressive BPV throttling was excluded due to the diminishing dilution level increase during RB ON and the risk of severely deteriorated turbocharger performance and excessing PMEP during active rebreathing after the mode-switch event.
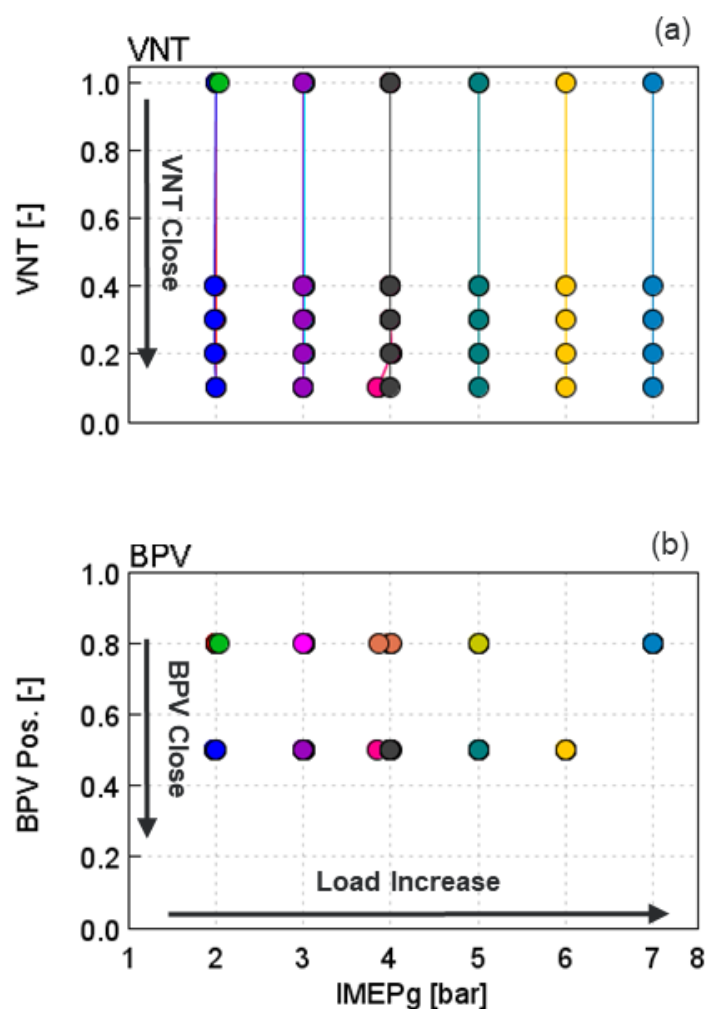
Figure 10. Parametric study range involving the (**a**) VNT position and (**b**) BPV position, conducted for both RB ON and RB OFF cases, at 1500 RPM.

Figure 11a,b shows the total in-cylinder dilution (RSG) and the (b) air–fuel ratio (AFR) trends, respectively, for both the RB ON and RB OFF cases, from the parametric sweeps. From Figure 11a, during RB ON, the RB*4 mm profile delivered nearly 50% RSG levels up to the 4 bar IMEPg. At 5 bar IMEPg, the dilution level distinctly dropped below the 30% level using the BPV position of 0.8 to avoid engine load compromise from excessive BPV throttling. For RB OFF, the RSG levels were reduced well below the 10% level, regardless of the VNT and BPV positions, across the IMEPg range of 1–7 bar.

From Figure 11b, increased trapped RSG, by using VNT closing during RB ON, reduced the total engine flow, thereby leading to a desirable AFR reduction trend and gas exchange losses, especially for IMEPg < 4 bar (shown in Figure 7a). At higher part load conditions (IMEPg > 5 bar), exhaust rebreathing was not needed due to adequate fueling and exhaust gas temperature. For RB OFF, increasingly closed VNT reduced these benefits due to the elevated total engine flow (AFR > 70) due to increased boost, as noted in Figure 11b. For the IMEP > 4 bar range, interestingly, increased fueling effectively achieved AFR in a desirable range (40 or below, an appropriate range after the RB mode-switch).

Moreover, Figure 12a,b shows the resulting TDC T and Exh T trends, respectively, for both RB ON and RB OFF cases, across the IMEPg 1–7 bar range. For a relative quantification of the thermal benefits, a minimum desirable TDC T of 905 K and Exh T of 573 K was estimated based on previous studies [22,27].
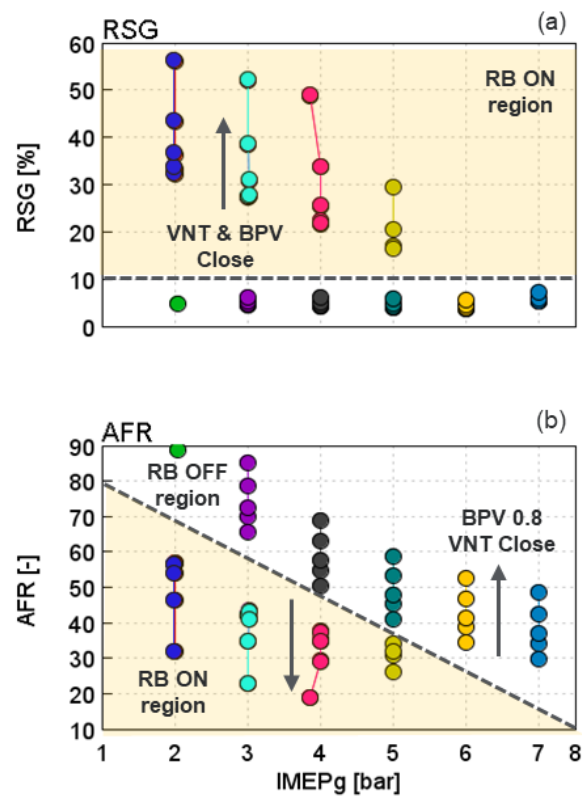
Figure 11. Comparison of (**a**) RSG and (**b**) AFR trends with respect to the VNT and BPV positions for both the RB ON and RB OFF cases.
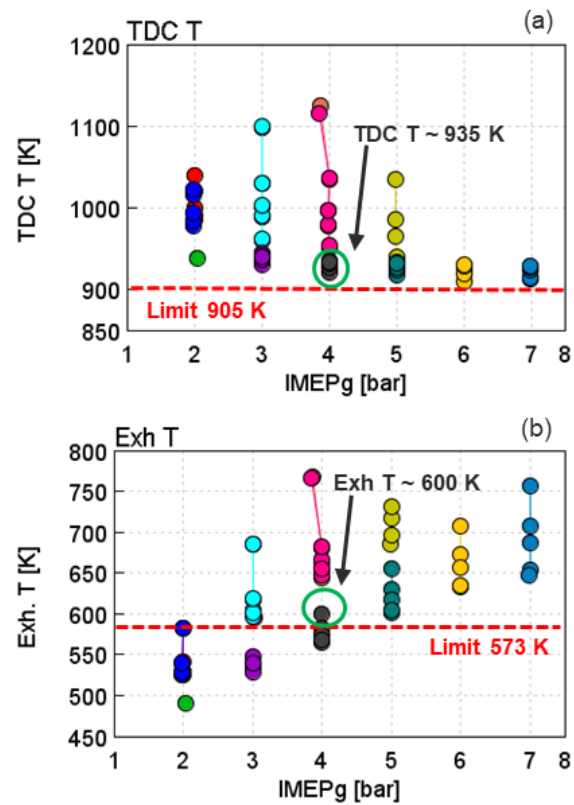

Figure 12. Comparison of (**a**) TDC T and (**b**) Exh T trends with respect to the VNT and BPV positions at different IMEPg (for IMEPg > 4 bar, only RB OFF data plotted).

For IMEPg up to 3 bar, the exhaust rebreathing successfully met the minimum TDC T (Figure 12a) and Exh T limits (Figure 12b); however, Exh T failed to meet the minimum requirement during RB OFF, due to the relatively much leaner air–fuel mixture (as noticed in Figure 11b). This indicated that mode-switch at light load conditions risk AT system performance due to low exhaust gas temperatures. On the other hand, for IMEPg above 5 bar, high TDC T and the Exh T levels were observed during RB OFF, indicating a risk of over promotion during RB ON if selected for mode-switch. Apparently, for the IMEPg range of 4–5 bar, both TDC T of 930 K and Exh T > 600 K were achievable during RB OFF due to the richer charger mixture (low AFR (as highlighted in Figure 11b) and the TDC T could be moderated via VNT and BPV relaxing to avoid excessive MPRR and NOx.

It should be noted that the mode-switch load range was a strong function of engine speed. At a lower engine speed, mode-switch at a higher load can be anticipated due to reduced risks of over thermal promotion. These study of these variations on mode-switch will be attempted in future experiments; therefore, they were excluded from the scope of the present work. Following the thermodynamic performance analysis, the RB*4 mm valve profile was analyzed for kinematics and stress loading criteria compliance with a supplier partner. As a result, a production feasible exhaust rebreathing "RB 4 mm" profile was generated that was confirmed to satisfy the design criteria. Subsequently, the re-designed "RB 4 mm" valve profile was used for the 1D transient analysis.

4.4. Transient RB Mode-Switch Strategy Evaluations

With increasing the engine load, the RB ON→OFF (mode-switch) strategy effectively mitigated the over thermal promotion of the cylinder charge; however, it presents challenges of high engine-out NOx and low exhaust gas temperatures in the absence of dilution. To meet the ultra-low NOx emissions requirements, cooled external EGR became a necessity that potentially offered two-fold benefits: first, it reduced the engine out NOx levels and second, it had high exhaust gas temperatures by reducing the air–fuel ratio. Therefore, in this section, at 1500/4, an appropriate load condition for RB mode-switch (discussed previously) exhaustive transient simulations was run to conceptualize a viable transient RB mode-switch (ON→OFF) strategy, including cooled external EGR.

Prior to the transient simulations, a full-factorial parametric study including the BPV, the VNT, the VIC, and the LPEGR valve positions was conducted using the steady-state 1D engine simulations. Here, 2D contours of the critical engine performance parameters such as the TDC T, AFR, RSG, Exh T, exhaust backpressure, combined turbocharger efficiency, and the external EGR rate were plotted under both the RB ON and the RB OFF conditions. Using the 2D contour plots, appropriate regions were identified that achieved the specific requirement for both RB ON and RB OFF cases, and seemed suitable for the ON→OFF transition and vice-verse. For a qualifying the transient RB ON→RB OFF (mode-switch) strategy, the following requirements were imposed (listed in the order of priority):

1. Strategy simplicity
2. Pressure difference reserve of 4 kPa across the LPEGR valve ΔP_{LPEGRV}
3. Exh T > 573 K
4. Low gas-exchange inefficiency

As an example, the 2D contour plots of TDC T with respect to BPV and VNT positions for the RB ON and RB OFF cases are plotted in Figure 13a,b, respectively. Here, at 1500/4, the TDC T level was noted to be above the minimum limit (905 K) across the entire map for both cases. First, the grayed region of the 2D contour maps were excluded based on the set constraints, such as BPV > 0.8 (due to inadequate exhaust back-pressure), during RB ON, whereas BPV that closed below the 20% position led to an excessively higher exhaust backpressure and deteriorated turbocharger performance. In addition, the region with the VNT open with more than 80% open (over > 0.8) was undesirable due to the low RSG level during RB ON and the low boost potential and additional VNT actuation during RB OFF. Following the imposed priority order and the constraints, P1-to-P5 regions were identified in the map (BPV and VNT combinations), which ensured a satisfactory engine performance,

including TDC T, as shown in Figure 13a,b, at 1500/4. For RB OFF, a ΔP_{LPEGRV} of 4 kPa region was estimated that required an aggressive BPV closing, thereby, compromising the viability of the P1 and P5 regions for mode-switch.
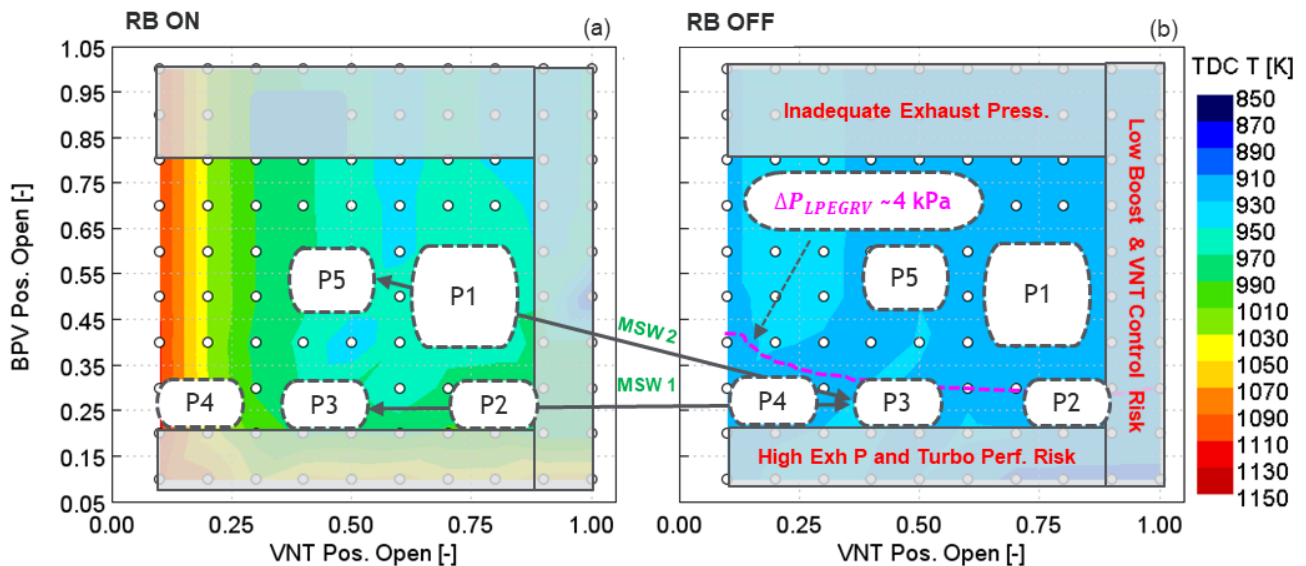

Figure 13. The 2D contour plots of TDC T for (**a**) RB ON and (**b**) RB OFF with respect to VNT and BPV positions using the RB 4 mm profile at 1500/4.

Using the steady-state map data, every possible combination of the highlighted regions for RB ON → RB OFF mode-switch, was analyzed. Table 3 provides a quick summary of each mode-switch strategy (MSW) in terms of its limitations and benefits. Most of the strategies were tagged as low-to-high risk for failing to meet the minimum pressure difference limit across the LPEGR.

From Table 3, out of the 25 mode-switch strategies shown, the RB mode-switch strategies termed as MSW 1 (P3→P3) and the MSW 2 (P5→P3) (also highlighted in Figure 13) were noted to have the most value. The MSW1 strategy met the TDC T and Exh T targets along with a high potential for ΔP_{LPEGRV}, with the simplest control strategy, thus showing the highest merit. On the other hand, the MSW 2 strategy, while meeting the TDC T and Exh T targets, offered PMEP reduction at the expense of increased control complexity, which could potentially be applied for mode-switch.

Subsequently, transient 1D engine simulations were performed to evaluate the effectiveness of the MSW1 strategy (P3→P3) at the 1500/4 engine condition. Prior to transient simulations, the engine model was imported with the supplier–provided turbocharger mass inertia data. The switch time from ON→OFF (translated from the response time of the hydraulically actuated oil flow control valve for the two-step exhaust valvetrain) was imposed as 100 ms (~1 engine cycle). For simulation, first, the estimated BPV, VNT, and total fueling for RB ON were imposed up to 5 s, followed by the RB ON→OFF transition only, representing the MSW 1 strategy, as shown in Figure 14a. Different positions and timing of the LPEGR valve opening (LPEGR 0–4 schemes), shown in Figure 14b, were incorporated with MSW 1 to examine the potential for cooled LPEGR delivery.

Table 3. Simulated RB mode-switch strategies and corresponding highlights at 1500/4.

| RB ON	RB OFF	Highlights/Concerns
P1	P1	Easy control, LPEGR ΔP limit
	P2	VNT open, not preferred for controls
	P3	BPV and VNT actuated
	P4	High AFR & PMEP
	P5	LPEGR ΔP criteria violation
P2	P1	LPEGR ΔP criteria violation
	P2	Controls met, VNT open, Increased BPV
	P3	VNT actuated, controls non-prefer
	P4	High AFR & PMEP
	P5	LPEGR ΔP criteria violation
P3	P1	LPEGR ΔP criteria violation
	P2	VNT ~FO, Increased BPV
	P3	**TDC T > 1173 K, Exh T ~ 573 K, Press. Promo, LPEGR available Controls met (MSW 1)**
	P4	High AFR & PMEP
	P5	LPEGR ΔP criteria violation
P4	P1	LPEGR ΔP criteria violation
	P2	VNT ~FO, Increased BPV
	P3	Performance met, BPV, VNT actuation
	P4	Controls met, High AFR & PMEP
	P5	LPEGR ΔP criteria violation
P5	P1	LPEGR ΔP criteria violation
	P2	VNT ~FO, Increased BPV
	P3	**TDC T > 1173 K, Exh T ~ 573 K, Press. Promo, LPEGR ΔP, low BSFC, addn'l BPV (MSW 2)**
	P4	Controls met, High AFR & PMEP
	P5	LPEGR ΔP criteria violation
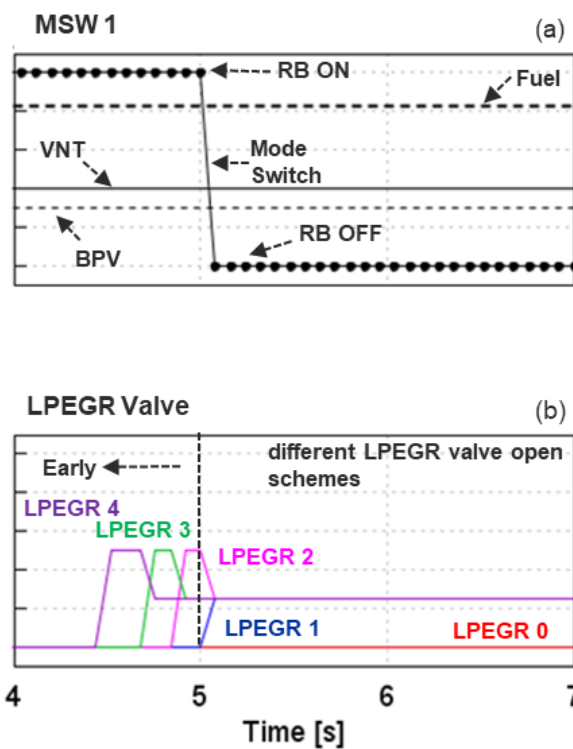
Figure 14. (**a**) Fueling, VNT, BPV, and RB positions for the MSW1 strategy correspond to (**b**) different LPEGR valve opening strategies investigated at 1500/4.

Figure 15a–f shows the response for the (a) total RSG level, (b) normalized engine-out NOx, (c) air–fuel ratio (AFR), (d) GOC space velocity, (e) BMEP, and (f) EGR rate for the MSW1 strategy, including different LPEGR schemes. It is evident from the figures that the cooled LPEGR flow during RB OFF significantly improved the RSG response and acceptable engine performance. The LPEGR 1 scheme, post RB ON→OFF switch, effectively increased the RSG level up to 25% (Figure 15a), thereby reducing the engine out NOx (Figure 15b) and air–fuel ratio (AFR ~45 from Figure 15c), compared with the LPEGR 0 scheme. As expected, a longer transport time of the external EGR from the LPEGR cooler out to the intake ports significantly spiked the engine-out NOx during the RB ON →OFF transition. Therefore, for a tighter NOx control advancing of LPEGR valve open time (relative to the mode switch time of 5 s shown in Figure 14b), the position and durations (LPEGR 2, LPEGR 3, and LPEGR 4) were expected to improve the NOx trends.
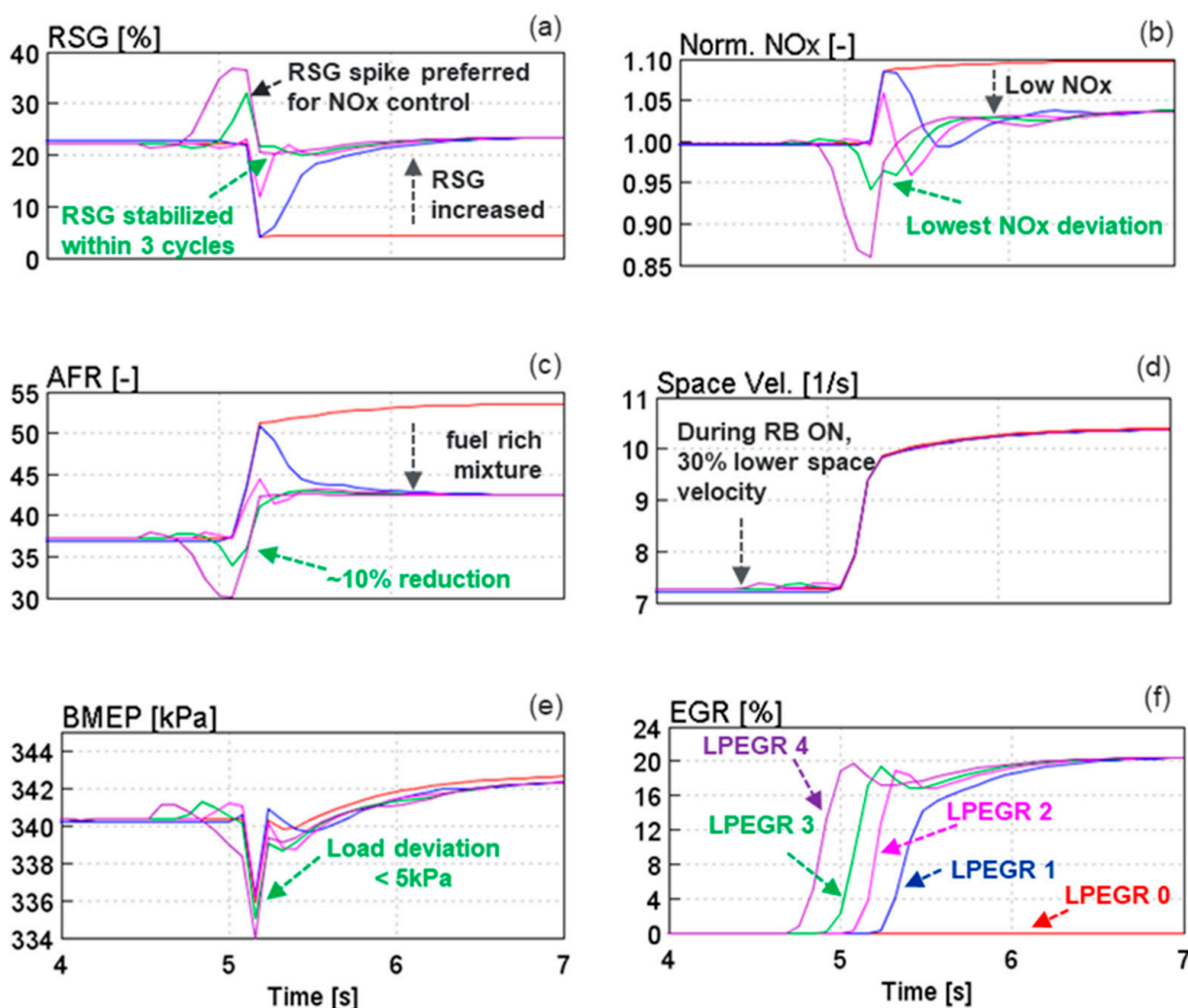

Figure 15. Comparisons of the (**a**) total RSG, (**b**) normalized NOx, (**c**) total engine air flow, (**d**) GOC space velocity, (**e**) BMEP, and (**f**) ext. EGR rate trends for different LPEGR valve cases, using the MSW1 mode-switch strategy at 1500/4.

These schemes, by significantly improving the total dilution level availability prior to the mode-switch (Figure 15f), effectively prevented spiked NOx trends, as noticed in Figure 15b. The LPEGR 3 scheme, using a 300 ms early opening of the LPEGR (to its 50% open position followed by its 25% open position) recovered the RSG level ~1 s faster than the LPEGR 1 scheme (Figure 15a), and demonstrated an acceptable deviation in RSG. Consequently, the response of the LPEGR 3 scheme effectively managed low AFR (~42) and reduced NOx (from Figure 15b). On the other hand, the LPEGR 4 scheme showed a higher

RSG deviation with an almost negligible benefit in the RSG recovery time (Figure 15a), whereas the LPEGR 2 scheme was noticed as an inadequate strategy to prevent spike in the NOx response during the mode-switch (Figure 15b).

Interestingly, with rebreathe on, the space velocity in the GOC catalyst was noted as being ~30% lower compared with the RB OFF case, as shown in Figure 15d. Low space velocity is known to be beneficial for the catalytic activity.

From Figure 15e, the deviation in BMEP trend was observed to be negligible with respect to the LPEGR schemes, which were primarily attributed to the fixed fueling strategy. However, a slower BMEP increase after RB OFF (time > 5.1 s) suggested turbocharger lag effect. To corroborate this, trends for the intake manifold pressure (IMP) and the turbocharger speed (TrbRPM) were plotted in Figure 16a,b, respectively.
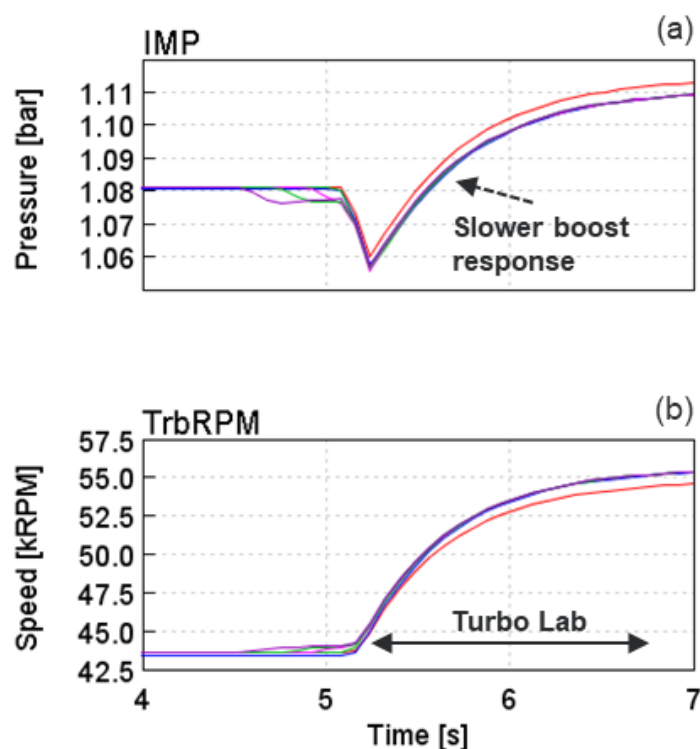

Figure 16. (**a**) intake manifold pressure and (**b**) turbine speed trends for the MSW1 strategy corresponding to different LPEGR valve opening strategies investigated at 1500/4.

After RB OFF and increased exhaust enthalpy at the turbine inlet, instantaneously, TrbRPM increased gradually owing to the turbine wheel and shaft assembly mass inertia. For 1500 RPM, the model predicted a ~2 s response time for achieving a steady-turbine speed after the mode-switch. Consequently, increasing the turbine speed raised the intake manifold pressure via compressor work, thereby proportionally increasing BMEP with a similar response (Figure 15e).

Furthermore, during mode-switch, the transition from rebreathing to cooled LPEGR for dilution increased, using the MSW 1 and the LPEGR 3 scheme, and the RSG imbalance among the cylinders were likely to be affected. Figure 17a compares the resulting in-cylinder RSG trends and Figure 17b shows the trends for the total CO_2 concentration (proportional to external EGR) in the exhaust manifold, the intake manifold, and the LPEGR cooler out location.
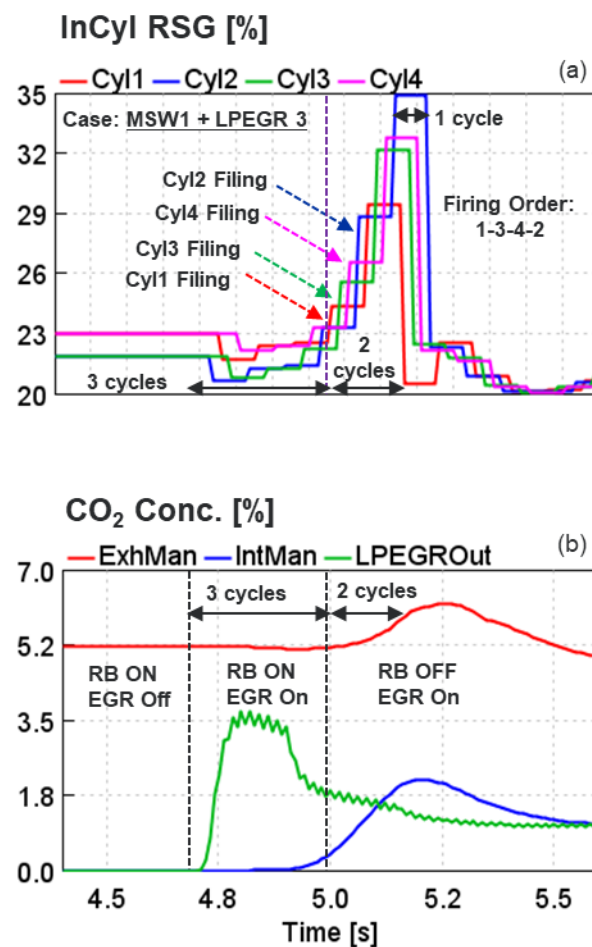
Figure 17. Transient trends of (**a**) the RSG level for Cyl 1 thru Cyl 4 and (**b**) CO_2 concentration trends in the exhaust manifold, the intake manifold, and at the LPEGR cooler out, using MSW1 + LPEGR 3 strategy.

From Figure 17a, prior to the mode-switch, (RB ON, t < 4.8 s), cylinders 1 and 4 (outer pair) showed a ~1.5% higher RSG level compared with cylinders 2 and 3 (inner pair) confirming the reasonably uniform RSG distribution among the cylinders for the rebreathing strategy. The CO_2 concentrations in the intake manifold and the LPEGR cooler out location were noted as being zero, during RB ON, as expected (Figure 17b).

Subsequently, during the t = 4.8–5 s range, with the LPEGR valve opening during RB ON, the in-cylinder RSG trends dipped instantaneously, as shown in Figure 17a. This was primarily caused by the reduced exhaust backpressure from the LPEGR valve opening. During this time, the in-cylinder residual trends marginally changed, as the CO_2 concentration in the intake manifold remained nearly zero, even when the CO_2 concentration at the LPEGR cooler out rapidly increased, as noted in Figure 17b.

Interestingly, after RB OFF (for t > 5 s), rising in-cylinder RSG levels indicated the arrival of external EGR into the cylinders, as confirmed by the increasing CO_2 concentration in the intake manifold (Figure 17b). From Figure 17a, distinct step-wise RSG trends were observed during cylinders filling after RB OFF. At 1500 RPM, t =5 s nearly synchronized with the beginning of the intake stroke of cylinder 1 and facilitated the filling of cylinder 1 with the cooled LPEGR flow first, followed by the rest of the cylinders in the order of firing. The magnitude of the step-wise RSG trend increased proportionally with the increasing availability of the CO_2 concentration in the intake manifold (Figure 17b). Interestingly, during the filling process, the RSG imbalance among the cylinders increased and managed a maximum RSG difference of ~6% (between cylinders 1 and 2) for the first two engine cycle period after t = 5 s.

Subsequently, one engine cycle later (t = 5.22 s), the RSG for cylinder 1 dropped below 20% from the reduced LPEGR valve position, while the cylinder 2 RSG level was still maintained at 35%, due to the firing order, showing the largest RSG imbalance in the 20% to 35% range among the cylinders, during RB OFF. Nevertheless, in the following engine cycle, the RSG trends nearly merged down to ~22% and stayed fairly balanced, for all of the four cylinders.

This data show implications of large RSG imbalance among the cylinders with increasingly advanced and high LPEGR valve positions during the mode-switch transition, supporting the argument for the necessity of a properly devised LPEGR valve strategy. This level of scrutiny is seldom reported due to the measurement challenges, and it is critical for understanding the inherent RSG imbalance challenges among the cylinders and for devising an appropriate mode-switch strategy.

4.5. Engine Tests

The re-breath system thus designed was fabricated and implemented on a test engine. Experiments were conducted to evaluate the system's performance at 1500 RPM/2 bar IMEPg operating conditions to evaluate the previously discussed modelling results, and thereafter detailed VNT sweeps were conducted at multiple operating loads at 1200 RPM to characterize the engine and the aftertreatment performance.

First, measurements with the active exhaust rebreathing were compared with the 1D model predictions at the 1500 RPM and 2 bar IMEPg condition. Figure 18a–f shows a 1-to-1 comparison of engine airflow, external EGR rate, exhaust manifold pressure (EMP), exhaust manifold temperature (EMT), intake manifold pressure (IMP), and intake manifold temperature (IMT), respectively. With similar intake conditions for IMP and IMT, the air flow and EGR rate trends in Figure 18a,b, respectively, showed a fair correlation between the experiments and the simulations. In the simulations, for LP EGR flow delivery, a pressure difference range of 3–4 kPa across the BPV was maintained, similar to the experiments. However, the model appeared to over-predict the exhaust manifold pressure (Figure 18c) and exhaust manifold temperature (18d) with the VNT closing. These over-predictions were partly attributed to the expected discrepancy in the model's in-cylinder HRR and the heat transfer prediction and potential differences in the rebreathe valve characteristics under unusually closed VNT positions (below 5%). Nevertheless, the 1D model correlated reasonably well with the experiments, thereby confirming its fidelity for the analysis results discussed in the previous sections.

The detailed 1200 RPM VNT sweep test results were discussed next. For a gross indicated mean effective pressure (IMEPg) in the range of 1 to 5 bar, the VNT position was swept from maximum open with acceptable combustion stability (COV < 3%) to maximum close with acceptable EO smoke and combustion noise due to over-promotion at each load condition. To maintain the engine-out NOx (EO NOx) below the 1.3 g/kWh level, cooled low-pressure exhaust gas recirculation was utilized by throttling the back-pressure valve, when needed.

To demonstrate the effectiveness of the rebreathe strategy, Figure 19a–f shows the 2D contour maps of the (a) engine-out (EO) NOx, (b) EO non-methane hydrocarbons (NMHC), (c), EO smoke, (d) tail-pipe (TP) NOx, (e) TP NMHC, and (f) gasoline oxidation catalyst (GOC) mid-brick temperature with respect to the VNT positions for IMEPg up to 5 bar at the 1500 rpm. The recorded data showed that increasingly closed VNT with reducing IMEPg was beneficial for combustion stability via increased internal thermal promotion. With the increasing engine load, the relaxed VNT position helps avoid combustion over-thermal promotion (discussed in the analysis section previously). For each load condition, a desirable VNT position range was identified for an acceptable engine performance. This produced a calibration line spanning the load range is referred to as the "desired calibration, as shown in Figure 19. Along this line, the engine out NOx (Figure 19a) and NMHC (Figure 19b) emissions were noted below 1.3 g/kWh, 5 g/kWh, respectively, while

the smoke (Figure 19c) was noted below 0.4 FSN in the load range (<3 bar IMEPg), where the engine was likely to operate use exhaust rebreathing.
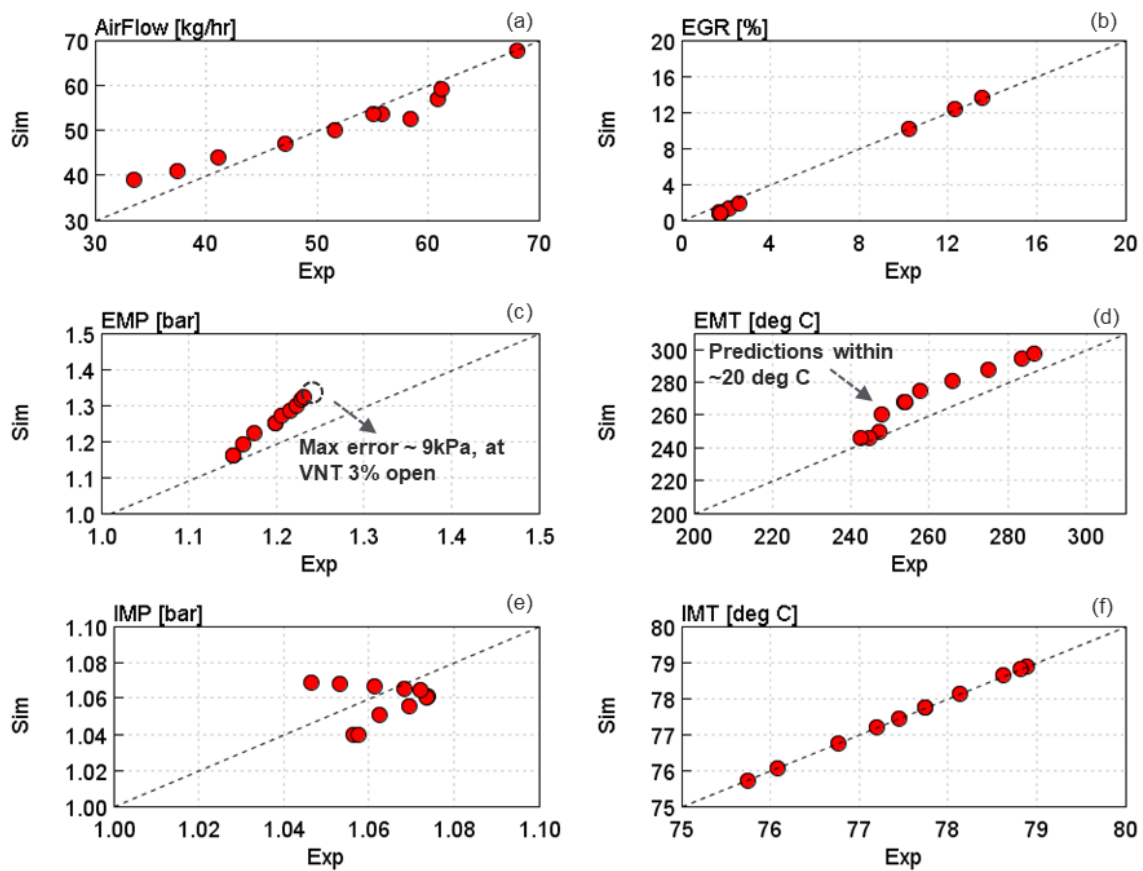

Figure 18. Comparison between the predictions and experiments for (**a**) air flow, (**b**) EGR rate, (**c**) exhaust manifold pressure (EMP), (**d**) exhaust manifold temperature (EMT), (**e**) intake manifold pressure (IMP), and (**f**) intake manifold temperature (IMT) at the 1500/2 condition.
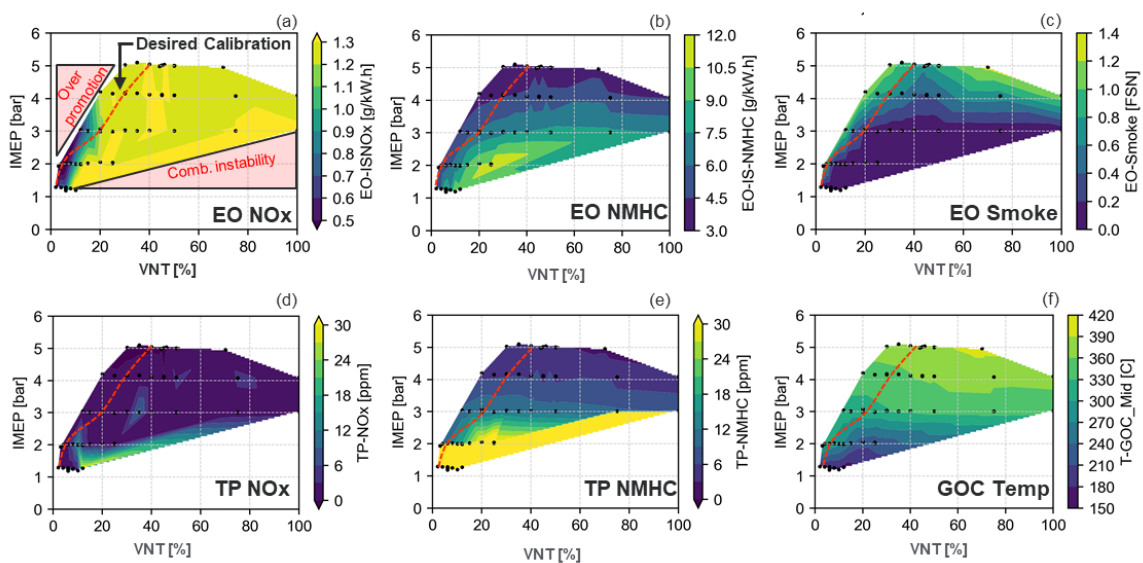

Figure 19. Measured 2D contour maps of (**a**) engine-out (EO) NOx, (**b**) EO non-methane hydrocarbons (NMHC), (**c**), EO smoke, (**d**) tail-pipe (TP) NOx, (**e**) TP NMHC, and (**f**) gasoline oxidation catalyst (GOC) mid-brick temperature at 1500 rpm.

With a favorable increase in the exhaust gas temperature, using exhaust rebreathing, the GOC mid-brick temperature was recorded in the range of 210 °C to 360 °C in Figure 19f. With a sufficiently high exhaust gas temperature in the after-treatment system, the tail-pipe (TP) NOx and NMHC emissions were recorded below 3 ppm and 30 ppm, as shown in Figure 19d,e, respectively. Finally, the tail-pipe smoke was recorded below 0.02 FSN, indicating near-zero tailpipe PM emissions.

To understand the effects of rebreathing on combustion, in-cylinder pressure and heat release traces were plotted for exhaust rebreathing off (RB OFF) and exhaust rebreathing on (RB ON), in Figure 20a,b, respectively, for the 1200/4.7 bar IMEPg condition. As expected, from Figure 20b, the peak cylinder pressure during the rebreathe event was noted as being ~7–8 bar lower than its counterpart, partly due to the low intake pressure and increased in-cylinder heat losses from the increased in-cylinder charge temperature. Nevertheless, the increased charge temperature helped reduce the deviation in the heat release, leading to a nearly identical pressure traces among the four cylinders, as shown in Figure 20b.
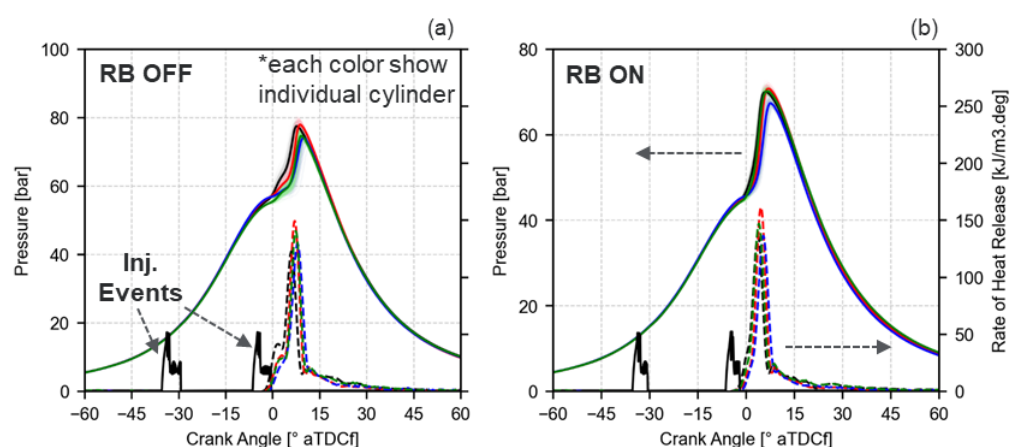

Figure 20. In-cylinder pressure and heat release traces for (**a**) rebreathing off (RB OFF) and (**b**) rebreathing on (RB ON) at the 1200 rpm and IMEPg 4.7 bar condition.

The key engine performance parameters for the test are tabulated in Table 4. The RB ON strategy demonstrated significantly improved brake specific fuel consumption, COV-IMEP, 55 °C increase in GOC mid-brick temperature, and ultra-low emissions for NOx, NMHC, and CO at the tail-pipe.

Table 4. Measured engine performance for RB OFF and RB ON at the 1200/4.7 condition.

	Measurements at 1200/4.7	
	RB OFF	**RB ON**
BSFC_ED [g/kWh]	222.6	**214.1**
IMP [kPag]	29	7
COV-IMEP [%]	1.3	**1**
Mid-GOC Temp [°C]	290	**346**
Mid-SCR Temp [°C]	285	331
EO NOx [g/kWh]	1.3	1.2
EO NMHC [g/kWh]	1.7	2.5
EO ISCO [g/kWh]	17	8
EO Smoke [FSN]	0.21	0.28
TP NOx [ppm]	1.6	**1.8**
TP NMHC [ppm]	15.3	**4**
TP ISCO [ppm]	0.7	**0.2**
TP Smoke [FSN]	0	**0.02**

Finally, preliminary transient mode-switch tests were performed at the 1200 rpm and the 4.7 bar IMEPg conditions. For these tests, numerous engine calibration iterations were conducted, including the fueling quantity split, injection timings, fuel rail pressure, external EGR levels, and VNT positions. For brevity of the manuscript, only the most relevant data are discussed in this section.

For these tests, first, stable engine conditions were maintained with RB OFF. Subsequently, rebreathing was turned-on by actuating the oil control valve that reduced the oil pressure in the rebreathe cam train, thus enabling RB ON. After achieving stable engine operation for RB ON, the rebreathing was turned-off. Figure 21a–f shows the trends for engine torque, combustion noise level (CNL), smoke, NOx, NMHC, and exhaust manifold temperature. For the RB OFF→RB ON transition (near the 38 s mark), elevated engine out NOx (Figure 21d) and CNL (Figure 21e) were visible, indicating advancing of combustion phasing with RB ON. The engine torque slightly dipped (Figure 21a) due to sudden over-dilution of the cylinder charge, which recovered quickly after the transition. Interestingly, from Figure 21f, the exhaust manifold temperature slightly dipped during the RB OFF→RB ON mode-switch event due to rebreathing of the exhaust gases from the exhaust manifold to the cylinder, which later followed a steady increasing trend facilitated by the richer combustion. For the RB ON→OFF mode-switch, trends were noted in reverse, as expected. Nevertheless, during this transient mode-switch testing, preliminary engine calibration optimization led to an acceptable range of CNL, emissions, and exhaust temperature levels.
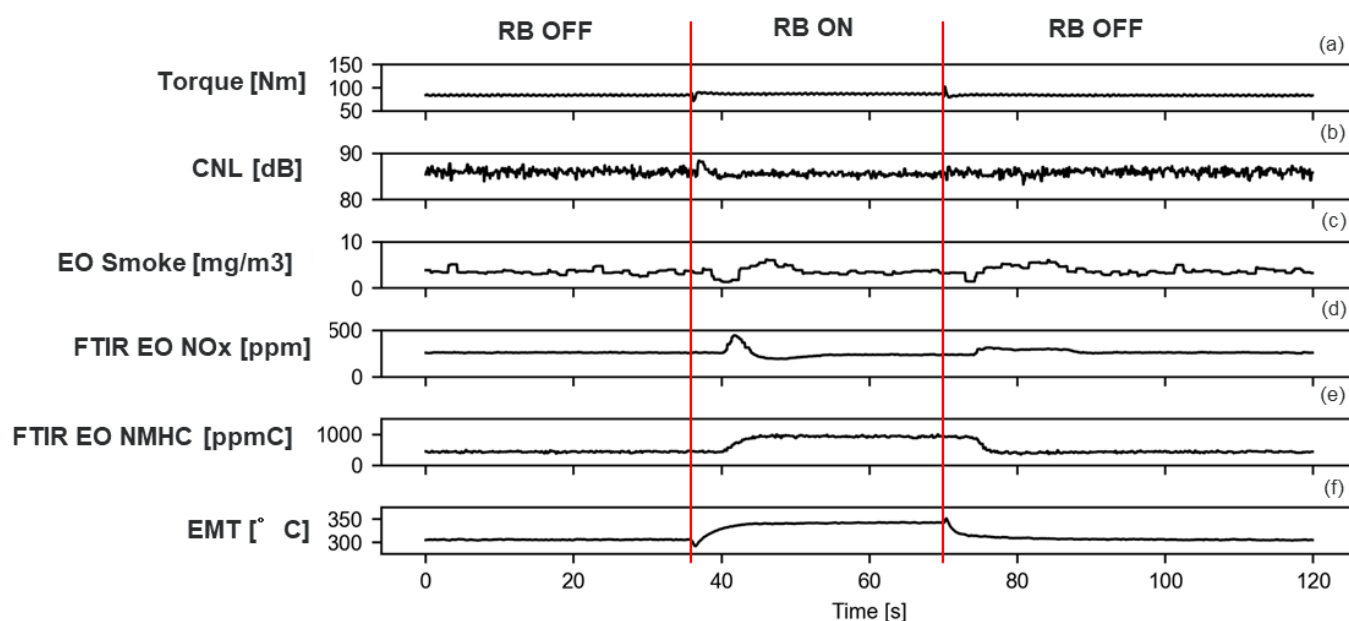

Figure 21. Trends for (**a**) engine torque, (**b**) combustion noise level (CNL), (**c**) EO smoke, (**d**) EO NOx, (**e**) EO NMHC, and (**f**) exhaust manifold temperature during mode switch at the 1200/4.7 condition.

5. Conclusions

A detailed numerical and experimental investigation was carried out to develop a two-step exhaust rebreathing strategy for the fuel-efficient thermal promotion of the cylinder charge and the exhaust gas at the low-load region for a prototype, low-NOx, four cylinder, 2.6 L, LDGCI engine. First, using a calibrated 1D engine model, simulations were conducted to fully characterize the exhaust rebreathing strategy potential over both steady-state and transient engine operations. An appropriate RB valve profile was identified for superior thermal performance, which also met the kinematic and dynamics stress limits. Furthermore, simulations were run to conceptualize a viable RB ON→OFF (mode-switch) strategy in the low-load region. Following the simulations, engine tests were conducted with the developed rebreathe cam to quantify the thermal benefits and emissions, and to further optimize the mode-switch strategy in the low-load regions. Moreover, experimental

data were found to reasonably correlate with the model predictions. The key conclusions from the study are the following:

1. The RB strategy, compared with EEVC, PVO, and NVO, demonstrated the highest fuel efficiency due to the lowest gas exchanges losses, at 650/1 and 1500/2 conditions.
2. Based on the simulations, an RB valve lift profile with the peak lift of 4 mm was designed that delivered superior thermal benefits.
3. For mode switching at 1200 rpm, a load range of 4–5 bar IMEPg was determined as being the most appropriate. RB ON was desirable up to 4.7 bar for thermal promotion.
4. Simulation-based transient mode switch strategies were conceptualized at the 1500/4 condition to minimize deviations in the dilution levels and to maintain an acceptable engine performance. An early opening of the LPEGR valve by 300 ms was noted as being the most advantageous for reducing lowering engine-out NOx, and minimized deviations in the engine load.
5. Steady-state testing of exhaust rebreathing showed low emissions and high GOC catalyst temperatures throughout the low-load region, primarily attributed to the effect of exhaust rebreathing. A desired engine calibration was identified that delivered EO NOx, EO NMHC, and EO smoke below 1.3 g/kWh, 3 g/kWh, and ~0.3 FSN, respectively.
6. Rebreathing demonstrated exhaust gas temperature above ~200 °C in the GOC at IMEPg 1 bar that steadily increased with the increasing load.
7. As a result of exhaust rebreathing and high exhaust temperatures, ultra-low tail-pipe emissions were recorded at the 1200 rpm and the 4.7 bar IMEPg condition.
8. The transient mode switch conducted at the 1200/4.7 condition demonstrated the benefits of the simultaneous use of rebreathing and external EGR for emission control. The refined engine calibration established a robust engine response, low CNL, high exhaust gas temperature, and low engine out emission emissions.

Abbreviations

AFR	Air fuel ratio
CAD	Crank angle degrees
CA50	Crank angle for 50% heat release
COV_{IMEP}	Coefficient of variance of IMEP
EGR	Exhaust gas recirculation
EO	Engine-out
EV	Exhaust valve
FSN	Filter smoke number
GCI	Gasoline compression Ignition
HRR	Heat release rate
IMP	Intake manifold pressure
IMT	Intake manifold temperature
IMEPg	Gross indicated mean effective pressure
IMEPn	Net indicated mean effective pressure
IV	Intake valve
MSW	Mode switch
NMHC	Non-methane hydrocarbon
NVO	Negative valve overlap
PMEP	Pumping mean effective pressure
PVO	Positive valve overlap
QSplit	Total fuel quantity split into injection events
RB	Exhaust rebreathing
RSG	Residual gas
SOI	Start of injection
TP	Tail pipe
VIC	Variable inlet compressor
VNT	Variable nozzle turbine
VVA	Variable valve actuation
10–90	Crank angle duration for 10–90% heat release

References

1. California Low-Emission Vehicle Regulations for Passenger Cars, Light-duty Trucks, and Medium Duty Vehicles. 1 October 2019. Available online: ww2.arb.ca.gov (accessed on 30 August 2022).
2. Regulation (EU) 2019/631 of the European Parliament and of the Council of 17 April 2019. Setting CO_2 Emission Performance Standards for New Passenger Cars and for New Light Commercial Vehicles; European Commission. Available online: https://ec.europa.eu/clima/policies/transport/vehicles/regulation (accessed on 30 August 2022).
3. China's Stage 6 Emission Standard for New Light-Duty Vehicles (Final Rule). The International Council on Clean Transportation (ICCT). Available online: https://theicct.org/sites/default/files/publications/China-LDV-Stage-6_Policy-Update_ICCT_2003 2017_vF_corrected.pdf (accessed on 30 August 2022).
4. Kalghatgi, G.; Risberg, P.; Ångström, H. *Advantages of Fuels with High Resistance to Auto-Ignition in Late-Injection, Low-Temperature, Compression Ignition Combustion*; SAE Technical Paper 2006-01-3385; SAE International: Warrendale, PA, USA, 2006. [CrossRef]
5. Kalghatgi, G.; Risberg, P.; Ångström, H. *Partially Pre-Mixed Auto-Ignition of Gasoline to Attain Low Smoke and Low NOx at High Load in a Compression Ignition Engine and Comparison with a Diesel Fuel*; SAE Technical Paper 2007-01-0006; SAE International: Warrendale, PA, USA, 2007. [CrossRef]
6. Kalghatgi, G.; Hildingsson, L.; Johansson, B. Low NO_x and low smoke operation of a diesel engine using gasoline-like fuels. *J. Eng. Gas Turbines Power* **2010**, *132*, 092803. [CrossRef]
7. Manente, V.; Zander, C.-G.; Johansson, B.; Tunestal, P.; Cannella, W. *An Advanced Internal Combustion Engine Concept for Low Emissions and High Efficiency from Idle to Max Load Using Gasoline Partially Premixed Combustion*; SAE Technical Paper 2010-01-2198; SAE International: Warrendale, PA, USA, 2010. [CrossRef]
8. Joo, S.M.; Alger, T.; Chadwell, C.; de Ojeda, W.; Zuehl, J.; Gukelberger, R. A high efficiency, dilute gasoline engine for the heavy-duty market. *SAE Int. J. Engines* **2012**, *5*, 1768–1789. [CrossRef]
9. Hoyer, K.; Sellnau, M.; Sinnamon, J.; Husted, H. Boost system development for gasoline direct-injection compression-ignition (GDCI). *SAE Int. J. Engines* **2013**, *6*, 815–826. [CrossRef]
10. Sellnau, M.; Foster, M.; Moore, W.; Sinnamon, J.; Hoyer, K.; Klemm, W. *Pathway to 50% Brake Thermal Efficiency Using Gasoline Direct Injection Compression Ignition*; SAE Technical Paper 2019-01-1154; SAE International: Warrendale, PA, USA, 2019. [CrossRef]
11. Cho, K.; Zhang, Y.; Cleary, D. Investigation of fuel effects on combustion characteristics of partially premixed compression ignition (PPCI) combustion mode at part-load operations. *SAE Int. J. Engines* **2018**, *11*, 1371–1383.

12. Sellnau, M.; Cho, K.; Zhang, A.; Cleary, D. Pathway to 50% brake thermal efficiency using gasoline direct injection compression ignition (GDCI). In Proceedings of the 28th Aachen Colloquium Automobile and Engine Technology, Aachen, Germany, 7–9 October 2019.

13. Zhang, Y.; Sellnau, M. *A Computational Investigation of PPCI-Diffusion Combustion Strategy at Full Load in a Light-Duty GCI Engine*; SAE Technical Paper 2021-01-0514; SAE International: Warrendale, PA, USA, 2021. [CrossRef]

14. Zhang, Y.; Kumar, P.; Traver, M.; Cleary, D. Conventional and low temperature combustion using naphtha fuels in a multi-cylinder heavy-duty diesel engine. *SAE Int. J. Engine* **2016**, *9*, 1021–1035. [CrossRef]

15. Zhang, Y.; Sommers, S.; Pei, Y.; Kumar, P.; Voice, A.; Traver, M.; Cleary, D. *Mixing-Controlled Combustion of Conventional and Higher Reactivity Gasolines in a Multi-Cylinder Heavy-Duty Compression Ignition Engine*; SAE Technical Paper 2017-01-0696; SAE International: Warrendale, PA, USA, 2017.

16. Zhang, Y.; Kumar, P.; Pei, Y.; Traver, M.; Cleary, D. *An Experimental and Computational Investigation of Gasoline Compression Ignition Using Conventional and Higher Reactivity Gasolines in a Multi-Cylinder Heavy-Duty Diesel Engine*; SAE Technical Paper 2018-01-0226; SAE International: Warrendale, PA, USA, 2018.

17. Deppenkemper, K.; Ehrly lng, M.; Schoenen, M.; Koetter, M. *Super Ultra-Low NO_X Emissions Under Extended RDE Conditions-Evaluation of Light-Off Strategies of Advanced Diesel Exhaust Aftertreatment Systems*; SAE Technical Paper 2019-01-0742; SAE International: Warrendale, PA, USA, 2019.

18. Kovacs, D.; Rauch, H.; Rezaei, R.; Huang, Y.; Harris, T. *Modeling Heavy-Duty Engine Thermal Management Technologies to Meet Future Cold Start Requirements*; SAE Technical Paper 2019-01-0731; SAE International: Warrendale, PA, USA, 2019.

19. Kumar, P.; Sellnau, M. *Evaluation of Fast Warm-Up Strategies for a Light-Duty Gasoline Compression Ignition (GCI) Engine*; SAE Technical Paper 2020-01-0317; SAE International: Warrendale, PA, USA, 2020.

20. Borgqvist, P.; Tunestal, P.; Johansson, B. *Gasoline Partially Premixed Combustion in a Light Duty Engine at Low-Load and Idle Operating Conditions*; SAE Technical Paper 2012-01-0687; SAE International: Warrendale, PA, USA, 2012.

21. Tanov, S.; Collin, R.; Johansson, B.; Tuner, M. Combustion stratification with partially premixed combustion, PPC, using NVO and split Injection in a LD-diesel engine. *SAE Int. J. Engines* **2014**, *7*, 1911–1919. [CrossRef]

22. Sellnau, M.; Sinnamon, J.; Hoyer, K.; Husted, H. Full-time gasoline direct-injection compression ignition (GDCI) for high efficiency and low NO_x and PM. *SAE Int. J. Engines* **2012**, *5*, 300–314. [CrossRef]

23. Zhang, X.; Wang, H.; Zheng, Z.; Reitz, R.; Yao, M. Experimental investigations of gasoline partially premixed combustion with an exhaust rebreathing valve strategy at low-loads. *Appl. Therm. Eng.* **2016**, *103*, 832–841. [CrossRef]

24. Andwari, A.M.; Aziz, A.A.; Said, M.F.M.; Latiff, Z.A. Experimental investigation of the influence of internal and external EGR on the combustion characteristics of a controlled auto-ignition two-stroke cycle engine. *Appl. Energy* **2014**, *134*, 1–10. [CrossRef]

25. Wu, H.W.; Hsu, T.T.; Fan, C.M.; He, P.H. Reduction of smoke, $PM_{2.5}$, and NO_x of a diesel engine integrated with methanol steam reformer recovering waste heat and cooled EGR. *Energy Convers. Manag.* **2018**, *172*, 567–578. [CrossRef]

26. Prasad, G. Strategies to control emissions from off-road diesel engines. In *Design and Development of Heavy Duty Diesel Engines*; Springer: Singapore, 2020; pp. 237–274.

27. Kumar, P.; Zhang, Y. Variable valve strategy evaluation for low-load operation in a heavy-duty gasoline compression ignition engine. *Energies* **2022**, *15*, 2017. [CrossRef]

28. *GT-Power Software*, GT-ISE version 2021; Gamma Technologies, Inc.: Westmont, IL, USA, 2021.

29. Kumar, P.; Sellnau, M. *EGR System Optimization for Light-Duty Gasoline Compression Ignition (GCI) Engine*; SAE Technical Paper 2021-01-0515; SAE International: Warrendale, PA, USA, 2021.